Dust Detection Using IR Channels of Himawari-8

Author

Keiko Yamamoto

A thesis submitted in partial fulfillment of

the requirements for the degree of

MASTER OF SCIENCE

(Atmospheric and Oceanic Sciences)

at the

UNIVERSITY OF WISCONSIN-MADISON

2016

Thesis Declaration and Approval

I, Keiko YAMAMOTO, declare that this thesis titled “Dust Detection Using IR Channels of Himawari-8” and the work presented in it are my own.

Keiko YAMAMOTO		
Author	Signature	Date

I hereby approve and recommend for acceptance this work in partial fulfillment of the requirements for the degree of Master of Science:

Steven A. Ackerman		
Committee Chair	Signature	Date
Andrew K. Heidinger		
Faculty Member	Signature	Date
Tristan S. L’Ecuyer		
Faculty Member	Signature	Date

Abstract

It was not until recently that both researchers and the public have found that dust, often referred to as yellow sand in Asia, can have a negative influence on daily life. For example, poor visibility caused by major dust storms can cause traffic disturbances and the fine dust particles can damage the human respiratory system. In order to monitor dust events, the use of algorithms using satellite data has been investigated. However, some algorithms currently used still have difficulty in detecting dust smoothly over land and ocean, or distinguishing dust especially during nighttime. In addition, some current algorithms involve using the visible or near infra-red channels, which means they can only monitor dust during daytime.

In this study, a new algorithm will be investigated that uses four infra-red channels, 8.6 μm, 10.4 μm, 11.2 μm, and 12.4 μm, on the Advanced Himawari Imager, which is on-board the Himawari-8 geostationary meteorological satellite. This algorithm was developed to detect dust all day over both land and ocean. The thresholds for this algorithm were empirically defined by using color information derived from two different Red-Green-Blue (RGB) images, RGB1 and RGB2. In RGB1, dust appears as orange to dark orange, with the land appearing as green. However, sometimes the land has dust-like feature, and it appears as dark orange. In RGB2, dust appears light green or pink, with land appearing as dark red. Because the color of land is different than the color of dust in RGB2, RGB2 will help clarify whether it is dust or land. By comparing to a previous three infra-red channel algorithm, it will be shown that the new algorithm can detect dust over the ocean as well and reduce the amount of false detection over the land during nighttime.

Acknowledgement

I had been working at Satellite Program Division at Japan Meteorological Agency and engaged in Himawari-8/9 project for more than three years before I came to Madison. Even though my tasks were mostly related to management things, my interest toward Satellite Meteorology got stronger and stronger each day. I cannot thank people enough for encouraging me and giving me the opportunity to study Satellite Meteorology at the University of Wisconsin-Madison, especially my family, my friends, my colleagues, and my professors. I wish to thank the Japan meteorological Agency and the Ministry of Land Infrastructure, Transport and Tourism for funding me.

I would like to express my sincere gratitude for Dr. Steve Ackerman and Dr. Andrew Heidinger for helping me come up with ideas on developing a new dust detection algorithm and teaching me how satellite meteorology plays a role in dust detection. I had never used IDL before engaging in this study, and I would like to express my deep gratitude for Yue Li, Steve Wanzong, Denis Botambekov, Yasuhiko Sumida, William Straka, and members in TC for helping me establishing the working environment, creating data set, and writing IDL codes. I wish to thank Dr. Grant Petty and Dr. Tristan L'Ecuyer for helping me go through my enrollment and graduation process.

It is famous in satellite communities in Japan as well that the University of Wisconsin-Madison is well-known for its top-notch education on Satellite Meteorology; however, it was not the only reason I decided to apply to the University. I had heard that Madison is a safe and sound city. I have lived here for almost two years and never had a scary experience. People are so nice and friendly, and despite the deadly cold winter, I feel

that I want to stay here. Fireflies, squirrels, rabbits, cardinals, gold finches, and all these cute little living things grab my heart and never let go. The air is so fresh thanks to beautiful trees and flowers. I have spent relaxing days immersing myself in wonderful nature in Madison. I must not forget for the rest of my life that Ian's Pizza and Five Guys made my day many times.

Polishing my English proficiency was also one of big reasons that I decided to study abroad. I would like to express how thankful I am to my friends in the AOS for having me in study groups and chit-chatting. I have been stimulated by my brilliant friends, and I am really glad that I have come this far. Speaking of improving my English proficiency, I wish to thank WESLI, an English second language institute in Madison, for teaching me grammars and slangs. I found that the knowledge of grammar is very important for non-native speakers to guess and understand what is written and spoken. I would also like to express my thanks to my private pronunciation teacher, David Letterman, Stephen Colbert, Jimmy Fallon, James Corden, John Oliver, Hamilton and American Ninja Warrior for helping me improve my listening and speaking skills. I try to speak English with American accent. I know many people consider British accent is prettier; however, since I fell in love with Stephen Colbert, it is a must to put my full effort to be able to speak like him.

The experience I have had in the United States of America is my precious asset. From now on, I will try to make the best use of it on my tasks at the Japan Meteorological Agency. Once again, thank you for helping me come this far.

Keiko Yamamoto

Madison, Wisconsin

May 2016

Table of contents

List of figures

List of tables

1. Introduction

It is widely known in Japan that yellow sand comes from the west, mostly in spring. Its traditional seasonal words such as “tsuchi-furu” (sand rains) have been used in literature for centuries. The arrival of yellow sand in Japan is known as the sign of the beginning of spring. While it sounds poetic and seems likely that the people welcome spring by looking at the hazy sky, research on the impacts brought by dust events including yellow sand has been done in recent years. Research has shown that dust events have a negative influence on daily life: poor visibility may cause traffic disturbances and particles could damage the respiratory system (see Section 2). These negative impacts are recognized by not only researchers in science and medical fields but people in the public as well. Since there has been an increasing interest from the public, several government agencies, such as the Japan Meteorological Agency (JMA) and the Japanese Ministry of Environment, have begun releasing information relevant to dust events.

Dust events are of interest to other geographic regions as well. According to the survey conducted in 2011 for the member countries of World Meteorological Organization (WMO) among Asia-Oceania regions (RA II Pilot Project, 2011), countries in these regions have a stronger interest in monitoring dust events than users in other regions of the world. Those users provide weather related information to the public every day, and they may know that the public wants them to release better information on dust events. Therefore, monitoring dust events is one of the essential tasks for these regional meteorological organizations.

One of the most effective ways to monitor dust is the usage of meteorological satellite data, in particular geostationary satellites. This is because geostationary satellite can provide temporal coverage of when dust events begin as well as spatial coverage showing how wide the event will cover. There has been much previous research on dust events developing dust detection algorithms from polar-orbiting satellite data. However, those algorithms have difficulty detecting dust over land and ocean, or distinguishing dust especially during nighttime. In addition, some algorithms that use visible channels can only monitor dust during daytime. The summary of this research is discussed in section 2.

The purpose of this study is to develop an algorithm to detect dust smoothly over land and ocean constantly for 24 hours. To do this, we have chosen to utilize the latest and most advanced imager in the region, the Advanced Himawari Imager (AHI). AHI is on the newest geostationary meteorological satellite, Himawari-8, which was launched in October 2014 by JMA, and became operational in July 2015. The 16 bands on the AHI instrument is expected to enhance the quality of monitoring dust over Asia-Oceania regions. AHI includes three IR channels which are well-known for their usefulness in detecting dust, and they are the 8.6 μm, 11.2 μm, and 12.4 μm channels. In addition, AHI also has a 10.4 μm channel, which will play an important role in the dust detection algorithm in this study, and will be introduced in the later chapter. This study will show that with those four IR channels alone, the new algorithm successfully detects dust over land and ocean around the clock.

2. Background

Before modern times, yellow sand was considered a seasonal phenomenon. It was not until recently that researchers have found that the particulate matter (PM) and other particles within the dust may cause health problems and air quality issues.

The transport of continental aerosols including yellow sand has been researched for a long time since it is believed to be one of the origins of the sediments in the ocean. Tsunogai and Kondo (1982) analyzed the aerosol samples collected in the surface air over the North Pacific and concluded that, even though the events occur sporadically, yellow sand contributes to the accumulation of aluminosilicate in the pelagic sediment. Iwasaka et al. (1983) stated that the long-range transport of aerosols had become a center of attention for researchers in chemical oceanography and geochemistry, and investigated the method to measure aerosols by using satellite images and calculating back-scatter coefficients derived from lidar observations. They observed an average horizontal dust area, and it was estimated at approximately 1.36×10^6 km^2. For researchers who have been trying to figure out the impact of dust on marine ecology, measuring and estimating the amount of dust are the key factors as much as detecting dust.

Eventually, yellow sand started gathering attention from researchers and the public because it could cause health problems. The Japanese government set air quality standards for $PM_{2.5}$ in 2009; however, particulate matter over East Asia brought by yellow sand has been investigated for a longer period of time as it has been discovered that particulate matter carries continental minerals. Lee et al. (2003) found that the concentration of PM_{10} increases largely during Asian dust, and so do the concentrations of

chemical species such as Al, Mg, Fe, Mn, Ca, Ni, and Cr. Mori et al. (2003) showed that, attached with fine and coarse particles, which are less than 2.5 μm in diameter and 2.5 μm to 10 μm in diameter, respectively, those chemical species are known to be carried for a long distance from the interior of China to Japan. Kim et al. (2001) focused on the visibility impairment in the city of Kwangju, Korea during yellow sand events and found that the concentration of PM_{10} was relatively larger than those of the fine particulate. The increase in the concentration of fine and coarse particles was also shown in Kim et al. (2002). They found that Asian dust events contribute to increase major crustal components in fine particle fraction when compared to non-Asian dust period within the Korean Peninsula and in the near-by Asian areas. Furthermore, they concluded that the particulate matter carries anthropogenic sulfate and marine aerosols as well as continental minerals. They stated that anthropogenic signatures had been found in the metallic distribution patterns in the study. Particulate matter carries not only chemical species but fungal spores as well. Yeo and Kim (2002) showed that, during Asian dust periods, hyphomycetes species were found on particulate matter sized from 1.1 μm to 2.1 μm while there were not any species found during periods without Asian dust events. Yeo and Kim (2002) mentioned that some spores may be potent toxins and carcinogens which might cause health problems.

Air quality issues brought by yellow sand have been investigated in Taiwan as well. According to the analysis done by Lin (2001), there was a sharp increase in PM_{10} concentration in spring 2000, and air quality was categorized as “Very Unhealthful” and “Hazardous” in north Taiwan. Lin (2001) concluded that observed yellow sand originated from Mongolia, the Gobi Desert and the Loess Plateau. Kwon et al. (2001) analyzed how unhealthful and hazardous events were, by looking at the causal association between daily

death counts and 28 dust days during 1995 to 1998. On those days, the concentrations of PM_{10} and the level of CO, NO_2, SO_2, and O_3 were higher than those on the control days, and the humidity was slightly lower. Kwon et al. (2001) concluded that the dust events could increase the death counts caused by cardiovascular and respiratory problems. For those researchers focusing on health problems, the concentration, the trajectory, and the detection of dust are essential factors that should be understood as well.

Ever since the dust events received public attention for causing health problems, monitoring those events has become an important mission for various meteorological organizations, particularly those where major events impact their countries. The identification and detection have been investigated in many studies (introduced in the following paragraphs). Data derived from ground based observations and satellite observation play an important role in this field since satellites can obtain the data uniformly over a wide region, especially over oceans while ground based observations get the data sporadically.

Fraser (1976) showed that the estimation of the dust mass of a vertical column can be done with using satellite nadir radiance 0.5-0.6, 0.6-0.7, 0.7-0.8, and 0.8-1.1 μm and a radiative transfer model. He stated that the characteristics of light that are scattered from aerosol types should further be studied to improve the analyses using satellite data since these are useful factors to identify dust. For example, Kaufman et al. (1997) showed that the reflectances at 0.49 and 0.66 μm can be estimated by using the reflectance at 2.2 μm. Since the influence of dust is small at 2.2 μm channel, the differences between observed reflectance at 0.49 and 0.66 μm channels and estimated reflectances at those derived from 2.2 μm channel could tell the presence of dust.

Tanré et al. (1997) developed a method to investigate the aerosol optical thickness and aerosol size distribution over oceans by using only three parameters derived from spectral radiances at 0.55 to 2.13 μm channels measured at the top of the atmosphere. However, those channels are visible and near-IR channels, which means that method only works during daytime hours. Qu et al. (2006) developed an normalized difference dust index NDDI $= (R_{2.13}-R_{0.469})/(R_{2.13} + R_{0.469})$, where R_n is the reflectance at the top of the atmosphere at n μm channel. It was found NDDI shows negative value over cloud, and it is less than 0.28 over the surface and larger than 0.28 over the Gobi Desert. This index can identify water or ice clouds and ground features. Qu et al. (2006) also found that when the brightness temperature at around 10.78-11.28 μm channel shows less than 275 K, those pixels indicate airborne sand and dust; in other words, the algorithm can separate the surface and airborne dust.

There have been some studies that have used information from only the IR channels. Ackerman (1989) found that the radiative temperature difference between 3.7 and 11 μm channels can be used to infer the optical depth of the dust layer. According to Ackerman (1989), the method can be used during nighttime as well. However, the accuracy of the nighttime detection is less sensitive when compared to the daytime case. This is likely due to the fact that while the 3.7 μm channel is near-IR channel, it does encompass part of the visible (solar) spectra. Similarly, Ellrod et al. (2003) developed a simple parameter to detect dust using brightness temperatures at 3.9, 10.7, and 12.0 μm channels. The parameter was defined as $B = C + m_1(BTD12\text{-}10.7) + m_2(BTD3.9\text{-}10.7)$, where B is output brightness temperature (K), C is a constant, m_1 and m_2 are scaling factors, and $BTDn\text{-}m$ means brightness temperature difference between n and m μm channels. Using the

parameter, it is possible to detect dust during daytime over land and oceans and at night over oceans. The sensitivity drops during nighttime; however, using the wavelength of 3.9 μm is helpful during daytime since there is strong solar reflectance there that helps to identify dust. Nevertheless, Ellrod et al. (2003) mention that false detection may occur near cirroform clouds, because the cloud reflects sunlight strongly as well. As in Ellorod et al. (2003), Qu and Hao (2007) used coefficients to define Thermal Dust Index (TD). They set $TD = c0 + c1*BT20 + c2*BT30 + c3*BT31 + c4*BT32$, where cn is coefficient and BTm is the brightness temperature at band m on MODIS, i.e., 20 is 3.660 - 3.840 μm channel, 30 is 9.580 - 9.880 μm channel, 31 is 10.780 - 11.280 μm channel, and 32 is 11.770 - 12.270 μm channel. They noted that band 20 had been used only during daytime and that further investigation should be done over land since they focused on dust events over the Atlantic Ocean in the study. Zhao et al. (2010) developed a dust and smoke detection algorithm using more than three channels. They used brightness temperatures and reflectances at 0.47, 0.64, 0.86, 1.38, 2.26, 3.9, 11.0, and 12.0 μm channels, making it possible to monitor dust and smoke over both land and ocean during daytime.

We have seen that, when using the reflectance for the threshold in a dust detection algorithm, the sensitivity of the dust detection during nighttime drops since the reflectance highly depends on sunlight. This means that those algorithms that use visible reflectances are only applicable during daytime. Because dust is transferred by the wind, which occurs at all times of day, researchers have tried using IR-only dust detection algorithms. The Meteorological Satellite Center of JMA has used two infrared channels on MTSAT-1R, an older JMA geostationary meteorological satellite, to monitor dust. Hashimoto and Ohkawara (2007) defined the yellow sand index as $100 \times \log(BT12/BT11) +$

c, where *c* is a constant and *BTn* is the brightness temperature at *n* μm channel. Using this yellow sand index and a cloud mask product, dust has been detected all day over land and ocean. However, it was noted that it is hard to detect dust if it is deposited on the surface or dispersed. Hashimoto and Ohkawara (2007) used only two channels for their study; however, if one could use 8.5 μm channel, which is a water vapor IR channel, a more accurate dust detection could be done. Ackerman and Strabala (1994) showed that the brightness temperature difference between 11 and 8.3 μm channels could be used to monitor stratospheric aerosols containing H_2SO_4 over the water. In addition, Ackerman (1997) investigated the use of infrared observations at 8.5, 11, and 12 μm channels for detecting dust in the troposphere. The algorithm demonstrated by Ackerman (1997) is simple because it only uses the brightness temperature differences between 11 and 12 μm (BTD11-12), and 8 and 11 μm (BTD8-11). The deeper the dust optical depth is, the larger the differences in BTD11-12 and BTD8-BT11. Ackerman (1997) also mentioned that to retrieve the optical depth over land, it is required to define the surface spectral emittance, which depends on vegetation and the moisture of the top soil. Similarly, Zhang et al. (2006) developed a dust detection algorithm using three MODIS thermal IR channels (Table 1). This algorithm makes it possible to monitor dust during both daytime and nighttime; however, it cannot detect dust over the

Thresholds for the identification algorithm for dust storm

Threshold	Mask flag	Description
BTD(11 − 12)<−0.5 and BTD(8 − 11)>0	1	Relative strong dust region
BTD(11 − 12)<−0.5 and BTD(8 − 11)<0	2	Relative weak dust region
BTD(11 − 12)>0 and BTD(8 − 11)>0	3	Ice cloud
BTD(11 − 12>0 and BTD(8 − 11)<0	4	Low cloud or surface
0>BTD(11 − 12)>−0.5	5	Uncertain region

Table 1 Thresholds for the identification algorithm for dust storm (Zhang et al., 2006)

ocean accurately (Hong, 2009). According to Hong (2009), Kim et al. (2008) showed the difficulty distinguishing the Asian dust over the Yellow Sea by the brightness temperature difference between 10.8 μm and 12 μm. Hong (2009) referred to Simpson et al. (2000) for explaining the difficulty, stating that the reason might be due to the lower level dust layer and water vapor because a high concentration of water vapor in the atmosphere may cancel out the reverse absorption effect of acid and other debris in volcanic plumes. Hong (2009) developed the algorithm that can detect dust over the ocean using the characteristic of surface reflectivity and polarizations from the clouds and dust particles, in addition to the brightness temperature difference and the optical depth; nevertheless, since the algorithm uses four channels from 3 μm to 12 μm on MTSAT-1R, it is necessary to investigate if it works well for nighttime cases.

The issue with using visible or near-infrared channels for the dust detection is that the accuracy drops for nighttime detection. This is because there is no sunlight reflected off the dust particles. In order to monitor dust during nighttime as well, IR channels are useful and helpful. In previous research, it was shown that the algorithm using three thermal-infrared channels whose wavelengths are around 8.5, 11, and 12 μm can detect dust well both during daytime and nighttime. However, using these three channels was shown to fail to identify dust over oceans. While Himawari-8 has 8.6 and 12.4 μm channels that are often used for detecting dust, it also has two channels around 11 μm that are 10.4 and 11.2 μm. By using these two channels, this may aid in detecting dust over oceans. In this study, a new algorithm has been built for dust detection using those four channels, which will make it possible to monitor dust over both land and ocean during both daytime and nighttime.

3. Data

3.1. Himawari-8 data

Himawari-8, a new geostationary meteorological satellite, was chosen for testing a new algorithm for detecting dust. It was launched in October 2014 by JMA, and started its test operation from January 2015. After post launch testing, Himawari-8 began operation in July 2015. While the MTSAT series, the former geostationary meteorological satellites of the Agency, had one visible channel and four infra-red channels, the Advanced Himawari Imager (AHI) on Himawari-8 carries six visible and near-infrared channels and 10 infrared channels. When it comes to dust detection using MTSAT series, the Agency has used two channels: 10.8 μm and 12.0 μm. AHI has 8.6 μm, which is a similar channel that MODIS carries and has been widely used for detecting dust. The 8.6 μm channel on AHI is also expected to improve the quality of the dust detection. AHI also has two channels that are close to 10.8 μm channel on MTSAT series: 10.4 μm and 11.2 μm channels. While close to the 10.8 μm channel on MTSAT, they do show slightly different features and play an important role in building the algorithm in this study. The goal for developing the new algorithm is to detect dust during both daytime and nighttime. Given that former research showed good results, 8.6 μm, 11.2 μm, and 12.4 μm channels were initially chosen. In the development of the algorithm, 10.4 μm channel was included as well.

With regard to identifying land or oceans, land class data derived from The Clouds from AVHRR Extended System (CLAVR-x) was used. CLAVR-x uses a land/sea mask derived from the NASA EOS project supplied static dataset as well as World Vector Shoreline data and DTED DEM data provided by NIMA (then DMA) and bathymetric data

provided by the oceanographic community. The land/ocean mask is stored in a 1 km geographic (geodetic) projection. The values of the Land/Ocean mask are as follows:

0 = Shallow ocean

1 = Land (Nothing else but land)

2 = Ocean coastlines and lake shorelines

3 = Shallow inland water

4 = Ephemeral water

5 = Deep inland water

6 = Moderate or continental ocean

7 = Deep ocean

In this study, 1, 2, 3, and 4 were defined as "land" and 0, 5, 6, and 7 were considered "ocean." The reason that shallow inland water and ephemeral water are included in land is that the area of those regions would be small, and there would be little problem to consider these as land, and smooth the detection. In addition, cloud mask was used to remove the amount of false detection, and the sensor zenith angle was used to eliminate the data in the peripheral of Himawari-8's observation range. This is because the size of the pixel at the edge of disk is much larger than closer to nadir.

Wave length [μm]	Himawari-8/9				MTSAT-1R/2	
	Band number	Spatial resolution at SSP [km]	Central wave length [μm]		Channel name	Spatial resolution at SSP [km]
			AHI-8 (Himawari-8)	AHI-9 (Himawari-9)		
0.47	1	1	0.47063	0.47059	-	-
0.51	2	1	0.51000	0.50993	-	-
0.64	3	0.5	0.63914	0.63972	VIS	1
0.86	4	1	0.85670	0.85668	-	-
1.6	5	2	1.6101	1.6065	-	-
2.3	6	2	2.2568	2.2570	-	-
3.9	7	2	3.8853	3.8289	IR4	4
6.2	8	2	6.2429	6.2479	IR3	4
6.9	9	2	6.9410	6.9555	-	-
7.3	10	2	7.3467	7.3437	-	-
8.6	11	2	8.5926	8.5936	-	-
9.6	12	2	9.6372	9.6274	-	-
10.4	13	2	10.4073	10.4074	IR1	4
11.2	14	2	11.2395	11.2080	-	-
12.4	15	2	12.3806	12.3648	IR2	4
13.3	16	2	13.2807	13.3107	-	-
Central wavelengths of the AHIs are "Moment center wavelength" (provided by Exelis). SSP : sub satellite point						

Table 2 Imager specifications for Himawari-8/9 and MTSAT series (The Meteorological Satellite Center of Japan Meteorological Agency)

3.2. Dust event cases

Since Himawari-8 started distributing its data from 2015, there have been several dust events over Asia. Dust events in Japan are summarized on webpages provided by JMA and are released on the dates when yellow sand was observed. Based on the released information, the days when yellow sand was observed in more than five

prefectures (a term for political regions used in Japan) were chosen up as candidates for dust event cases.

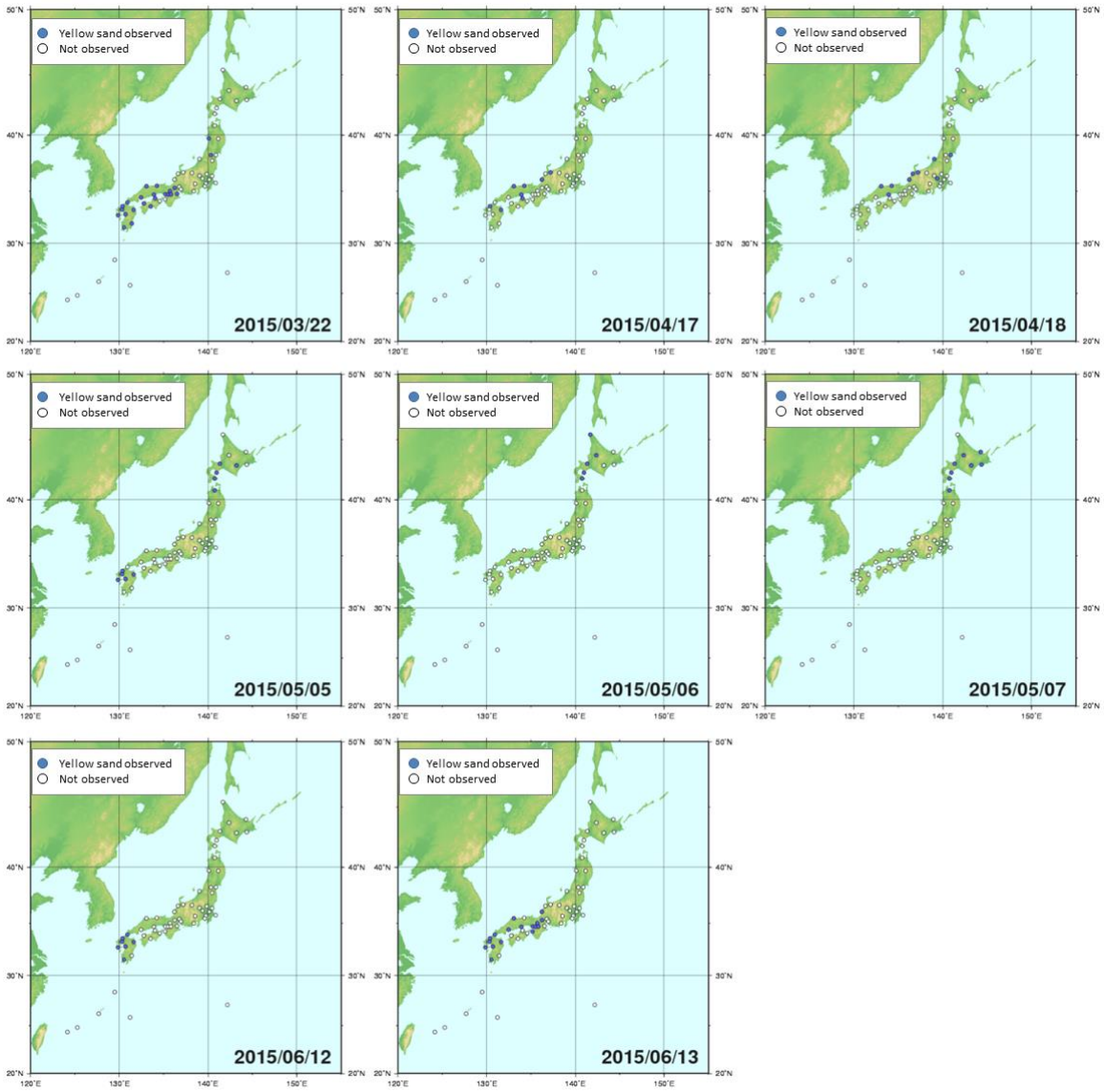

Figure 1 Dates when yellow sand was observed in more than 5 prefectures in Japan in 2015.

During the development of the dust detection algorithm, it was found that sometimes dust was too thin to be observed by satellites despite being observed by ground based observation. Considering the yellow sand observed cases introduced in Figure 1 and satellite images, six cases were chosen during 2015 to build the dust detection algorithm,

March 22, April 16 and 17, May 5 and 6, and June 9. In addition, a dust event that happened on April 27, 2015 over the west part of China was also chosen based on a news article released by chinadailyasia.com.

Most of those dust events were confirmed with visible composite images derived from Terra and Aqua MODIS using images from the NASA's Level 1 and Atmospheric Archive and Distribution System (LAADS) Web.

The summary of the data that was used to build the new dust detection algorithm is shown in Table 3. Since the focused region is Asia in this study, the area of the data is narrowed down to 30^{o} to 50^{o} N and 80^{o} to 150^{o} E.

Satellite	Himawari-8
Imager	Advanced Himawari Imager (AHI)
Wavelengths	8.6, 10.4, 11.2, and 12.4 μm
CLAVR-x data	land_class, cloud_mask, sensor_zenith_angle, surface_temperature_retrieved
Date	3/22, 4/16-17, 4/27, 5/5-6, and 6/9, 2015
Region	30^{o}-50^{o} N, 80^{o}-150^{o} E (Asia)

Table 3 Data used for building the algorithm

It should be noted that AHI started operation on July 7, 2015. Data prior to operations beginning is considered the post-launch checkout test period (PLT) where validation and changes to the calibration of the instrument take place. Because the events took place during PLT, it is possible that some of the algorithm thresholds may need to be adjusted slightly.

4. Dust Detection Algorithm

4.1. Basic RGB images

It is known that using three tones of light - red, green, and blue - makes it easier for us to see what types of clouds we look at on satellite images. The same three tones of light enable us to see dust as well. Martínez et al. (2009) introduced the parameters and these ranges for dust RGB composition using the data from Meteosat Second Generation (MSG) as in Table 4.

RGB color plane	Parameters: Brightness temperature (differences)	MIN	MAX
Red	12.0 μm – 10.8 μm	-4 K	+2 K
Green	10.8 μm – 8.7 μm	0 K	+15 K
Blue	10.8 μm	261 K	289 K

Table 4 Dust RGB composition for MSG (From Martínez et al., 2009)

Channels used in Table 4 are similar to those used in Zhang et al. (2006). With these parameters and ranges, the RGB image makes it possible for human eyes to identify dust, thin cirrus, and contrails. Figure 2 shows a dust event that happened over the Sahara desert in March 2004. The dust area is colored in pink or dark pink, suggesting that Red is positive, Green is around or less than 0 K, and Blue is around 275 K.

The reason why dust area is colored in pink or dark pink can be understood by looking at the features of parameters in Table 4. The brightness temperature difference between around 11 μm and 12 μm is helpful discriminate atmospheric constituent (McClain et al., 1985). In fact, the difference between 10.8 μm and 12.0 μm shows negative value in aerosol regions (Prata, 1989, and Ackerman, 1997). Since the parameter of Red is

12.0 μm – 10.8 μm, Red shows positive value in aerosol regions in Table 4. Ackerman and Strabala (1994) stated that the effect of the Mount Pinatubo aerosol on the brightness temperature difference between 8 μm and 11 μm is 1 to 1.5 K. The parameter for Green is 10.8 μm – 8.7 μm, so it would take small negative value when there is dust in Table 4. Ackerman and Strabala (1994) also stated that using three channels, 8 μm, 11 μm, and 12 μm is useful to distinguish aerosol from water vapor since water vapor increase leads the decrease in the brightness temperature difference between 8 μm and 11 μm while it leads the increase in the difference between 11 μm and 12 μm.

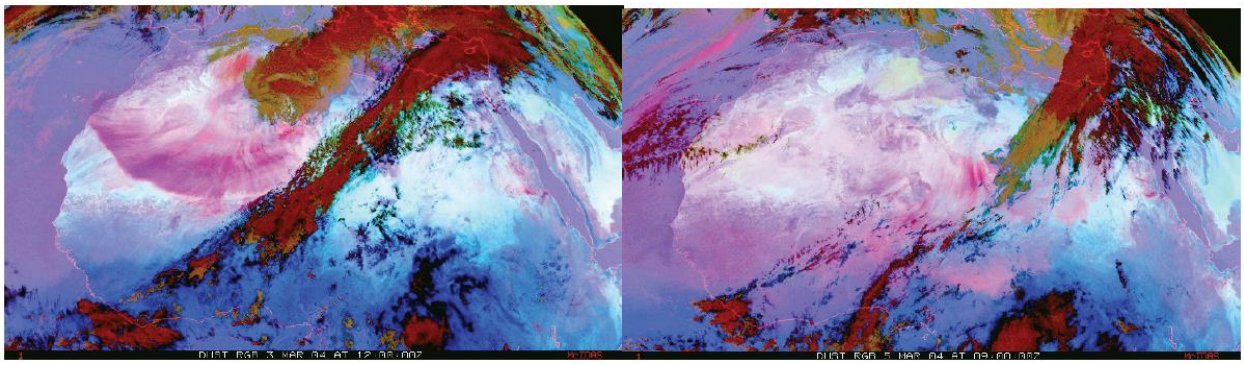

Figure 2 Dust RGB images during March 2004 dust event. 3rd March 2004 12Z (left) and 5th March 2004 9Z (right), from Martínez et al., 2009.

Dust over land can be easily identified with the RGB composition. However, dust over the ocean cannot be seen. As in Hong (2009), the algorithm introduced in Zhang et al. (2006) cannot detect dust over the ocean either parameters (see section 2), hence, it can be said that these three channels alone are not enough to detect dust over both land and ocean. Even though it does not detect dust over the ocean, both Zhang et al. (2006) and Martínez et al. (2009) showed fine results for detecting dust using three infrared channels around 8.5, 11, and 12 μm. These results were taken into consideration in this study, and it was

decided to use the similar 3 channels for the first parameters for RGB composition to develop the new algorithm. Since Himawari-8 does not have exactly the same channels as MSG does, those thresholds were modified to fit with the data of Himawari-8 (see the next section). Hereafter, the RGB image using the modified thresholds is called RGB1. Since it has been shown that there is a limit in detecting dust using just one RGB composition, for it cannot detect dust over oceans, another RGB composition called RGB2 was empirically defined to build the new algorithm, making it possible to detect dust over both land and ocean for a full day.

4.1.1. RGB1

For detecting dust, Zhang et al. (2006) used 8.5, 11, and 12 μm channels and Martínez et al. (2009) used 8.7, 10.8, and 12 μm channels and showed fine results. Considering these wavelenthgs, it was decided to use 8.6, 11.2, and 12.4 μm channels that Himawari-8 carries for drawing RGB1. The parameters and the ranges for red (R1), green (G1), and blue (B1) colors are shown in Table 5.

RGB color plane	Parameters: Brightness temperature (differences)	MIN	MAX
R1	12.4 μm – 11.2 μm	-4 K	+2 K
G1	11.2 μm – 8.6 μm	-4 K	+5 K
B1	8.6 μm	208 K	243 K

Table 5 Dust RGB composition parameters for Himawari-8 (RGB1)

When drawing RGB1, the color bar was inversed for B1. Hence, blue color 0 represents 243 K and blue color 255 represents 208 K. Since R1 should be positive and G1 should be around 0 K or less than that over aerosol regions (see section 4.1) and B1 is more than 243 K, dust is orange to dark orange in RGB1. When it comes to land surface, it shows

bright green color during daytime and it gets dark orange during nighttime. This may be because less water vapor leads the decrease in R1 and the increase in G1 (Ackerman and Strabala, 1994).

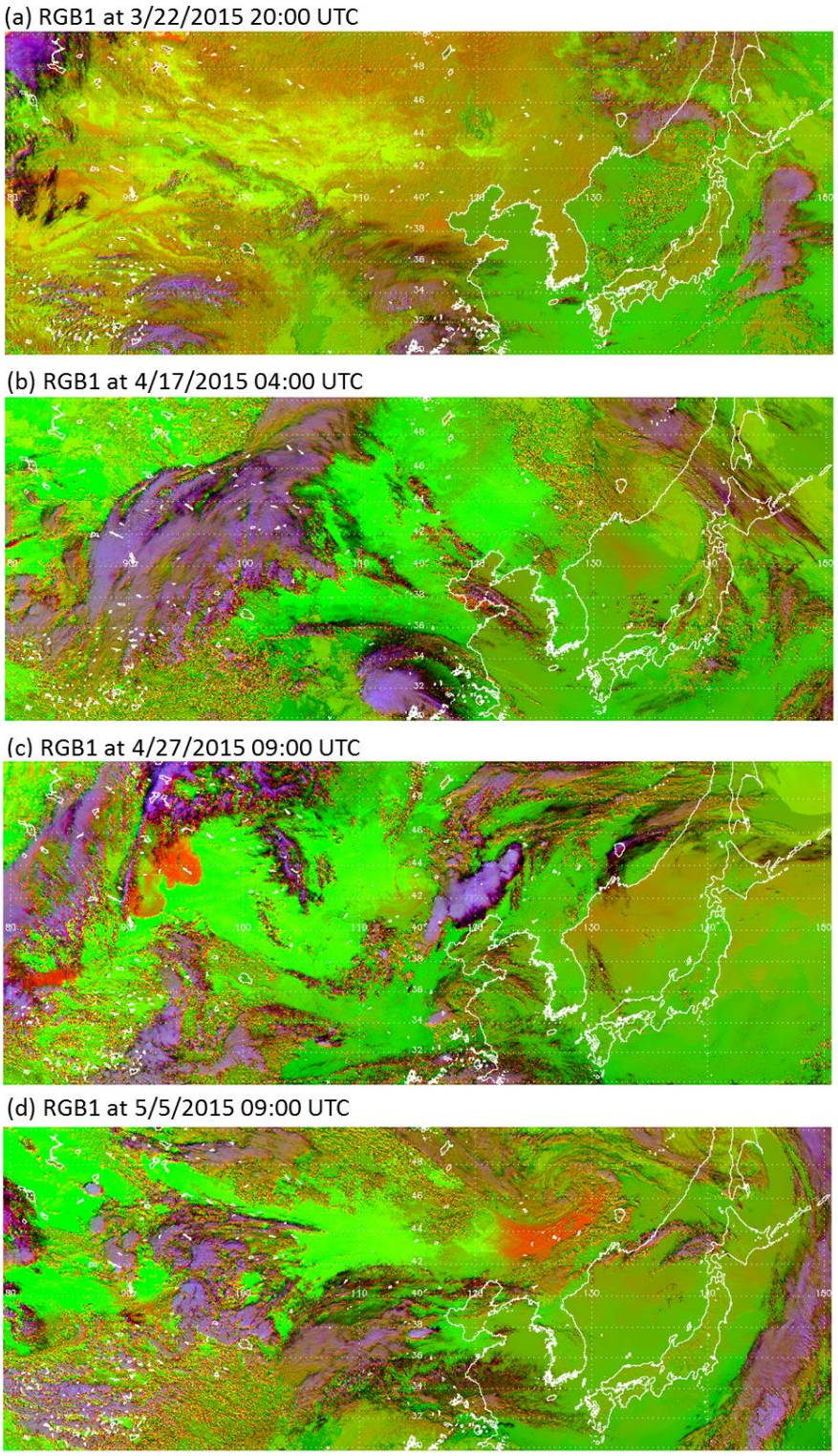

Figure 3 RGB1 images for (a) 3/22/2015 at 20 UTC, (b) 4/17/2015 at 4 UTC, (c) 4/27/2015 at 9 UTC, and (d) 5/5/2015 at 9 UTC. No dust on (a). Orange to pink plumes such as west part of Asia on (c) and east part of China (d), and dark orange plume over Sea of Japan on (b) are dust.

Figure 3 (a) is the image when there was no dust. It was midnight in local time, and land surface is more orange than that on Figure 3 (b), which is the daytime image, and land surface is bright light green during daytime. When dust has not dispersed yet, dust shows orange to pink color (Figure 3 (c) and (d)) while the cloud shows the color that includes blue, so it is easy to distinguish dust from clouds; however, when dust has been dispersed, it shows dark orange color like the plume over the Sea of Japan on Figure 3 (b). This color is similar to land surfaces or sea at times, making it hard to identify whether it is dust or not.

While it is hard to tell the difference between the land surface or sea and thin dust by staring at still images, it is easy to tell by looking at animations. When animating the imagery, the land and ocean remain stationary while the dust moves. This can be seen when looking at the dark orange plumes in Figure 3 (b), (c), and (d) over the Sea of Japan. One can observe that the plume on Figure 3 (b) moves as time passes, meaning it can be identified as dust.

4.1.2. RGB2

In order to distinguish dust from the land surface that shows dust-like features, and to make it possible to detect dust over the ocean, some new parameters were defined for red (R2), green (G2), and blue (B2) for the second dust RGB composition called RGB2 (Table 6). Due to the fact that the brightness temperature difference between around 11 μm and 12 μm plays an important role in distinguishing aerosol as in McClain et al. (1985), R2 is set the same as R1. Since G2 and B2 use ratios for their parameters, it is considered to be a missing value when the denominator is zero.

RGB color plane	Parameters: Brightness temperature (difference or ratios)	MIN	MAX
R2	12.4 μm – 11.2 μm	-4 K	+2 K
G2	(11.2 μm - 10.4 μm)/(12.4 μm - 8.6 μm)	-1	+2
B2	8.6 μm/11.2 μm	0.97	1.01

Table 6 Parameters for RGB2, a new dust RGB composition

When drawing RGB2, the color bar was inversed for B1 as in RGB1. In RGB2, land surface shows dark red color during nighttime (Figure 4 (a)) and dark green during daytime (Figure 4 (b)); on the other hand, dust shows pink or light green. For example, Figure 4 (c) is the image when a huge dust event happened over the west part of China, and pink plumes are noticeable on the image. Figure 4 (d) shows when dust event happened over the northeast of China, and light green plume can be seen. Figure 4 (b) is the image that shows dispersed dust over Sea of Japan, and the plume is darker than light green. These images suggest that dust mainly shows light green color and sometimes shows pink color in RGB2.

The color of dust in RGB2 is different from the land surface or sea with dust-like features in RGB1. In other words, RGB2 can distinguish dust and the land surface or sea with dust-like features quite well while RGB1 cannot; hence, using both RGB1 and RGB2 makes it possible to detect dust more accurately. This will be introduced in Section 5, which discusses the results of the comparisons and algorithm detection.

It should be noted that the physics behind G2 and B2 is needed to be investigated to explain why RGB2 successfully distinguish dust and dust-like regions.

(a) RGB2 at 3/22/2015 20:00 UTC

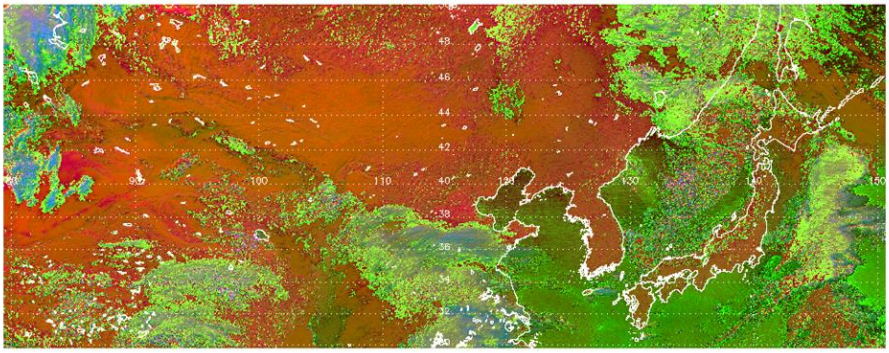

(b) RGB2 at 4/17/2015 04:00 UTC

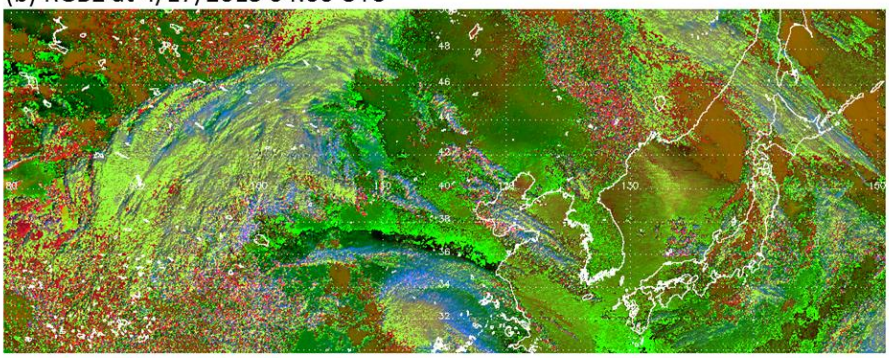

(c) RGB2 at 4/27/2015 09:00 UTC

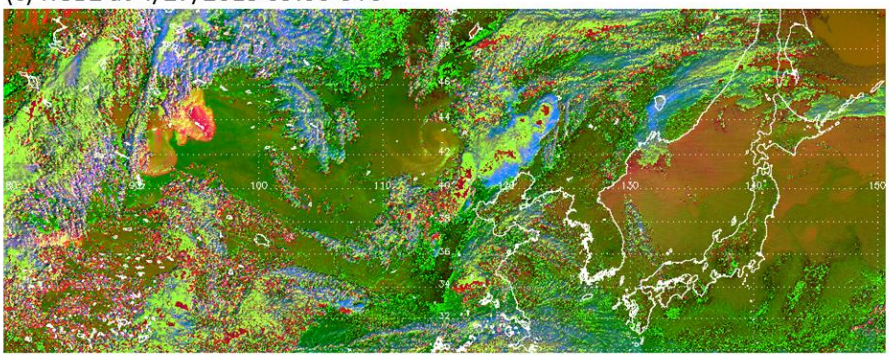

(d) RGB2 at 5/5/2015 09:00 UTC

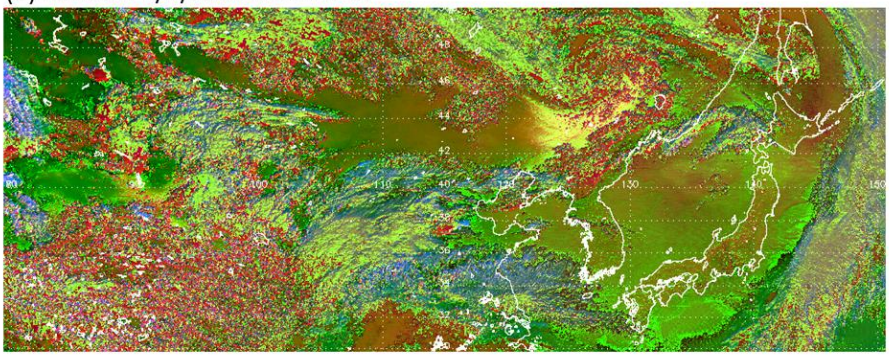

Figure 4 RGB2 images for (a) 3/22/2015 at 20 UTC, (b) 4/17/2015 at 4 UTC, (c) 4/27/2015 at 9 UTC, and (d) 5/5/2015 at 9 UTC. No dust on (a). Light green plumes such as over Sea of Japan on (b) and east part of China on (d), and pink plumes over west part of Asia on (c) are dust.

4.2. Comparison of the MODIS, RGB1, and RGB2

Before going into detail on the dust detection algorithm, a comparison among MODIS images, RGB1 images, and RGB2 images are performed. This is to see if dust is captured in the MODIS, RGB1, and RGB2.

4.2.1. March 22, 2015 case

(a) MODIS

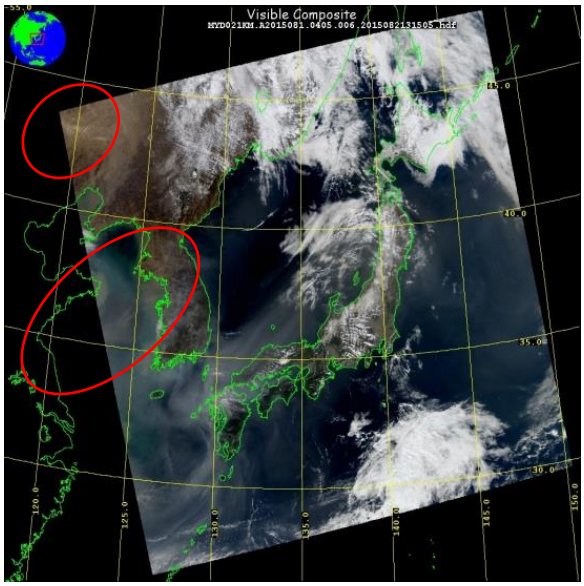

(b) RGB1

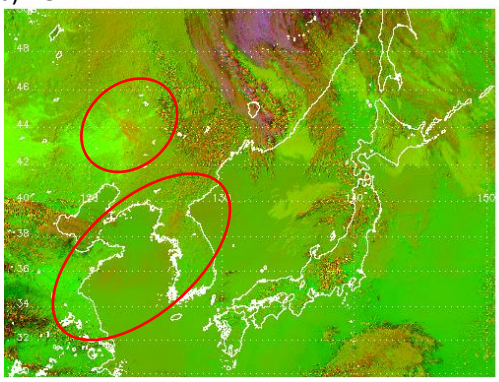

(c) RGB2

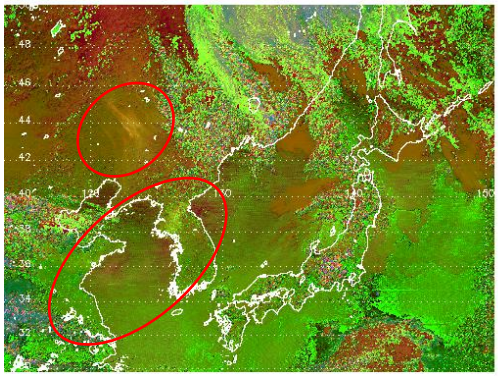

Figure 5 (a) MODIS image on 3/22/2015, 04:05 UTC. (b) and (c) RGB1 and RGB2 images on 3/22/2015, 04:00 UTC, respectively.

Small dust events happened over the East China Sea and northeast of China on March 22, 2015. It seems likely that MODIS passed over the regions after dust was dispersed, and it is a little bit difficult to identify dust on MODIS image (Figure 5 (a)) since the color of dust is so faint. In RGB1 (Figure 5 (b)), even the color is not outstanding, both dust plumes can be seen. In RGB2 (Figure 5 (c)), dust over northeast part of China and over

Korean Peninsula can be seen; however, dust over the East China Sea is not shown. This shows that as dust disperses, it gets harder to capture. Since AHI is on a geostationary satellite and it takes Full Disk data every 10 minutes, it is easy to see the motion of the dust by creating animation of RGB1 or RGB2. By watching the animation helps a lot to identify dust especially for the thin dust case, such as March 22. As dust gets thinner, it shows the similar color as some part of land surfaces, making it difficult to distinguish by looking at a still image.

4.2.2. April 16 and 17, 2015 cases

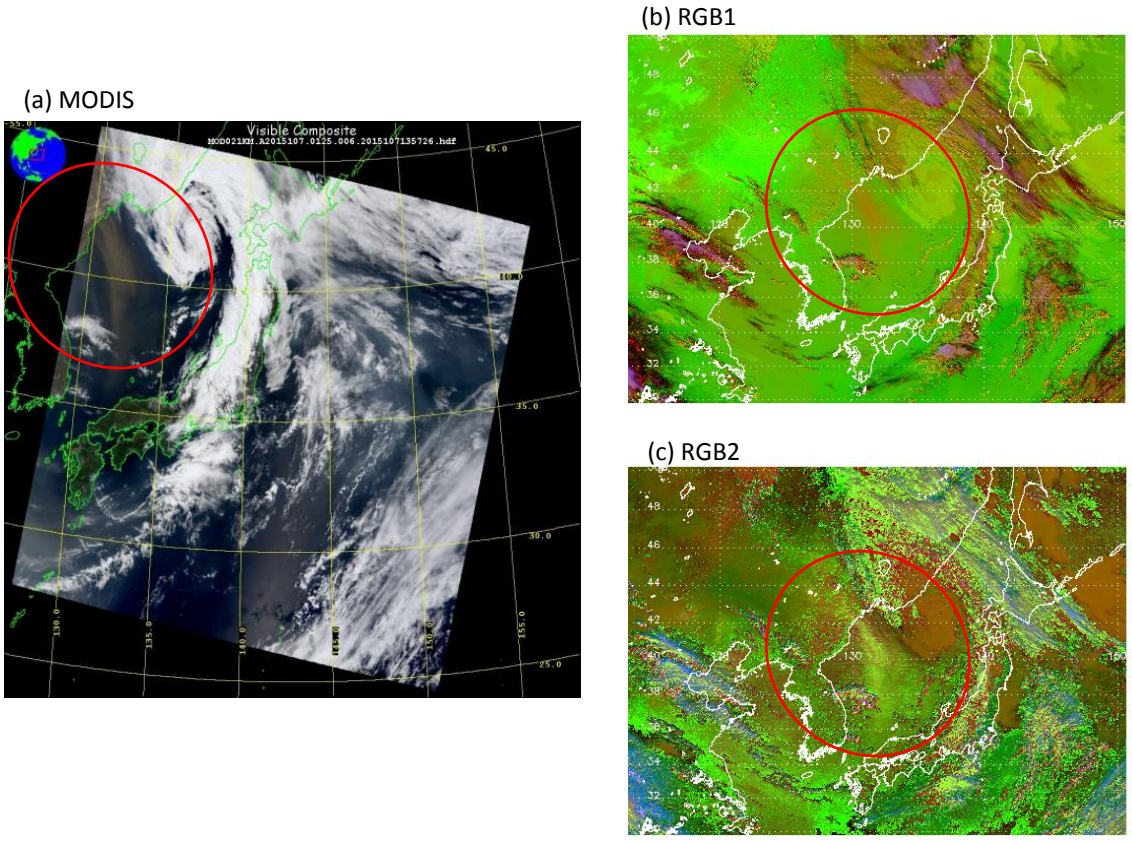

Figure 6 (a) MODIS image on 4/17/2015, 01:25 UTC. (b) and (c) RGB1 and RGB2 images on 4/17/2015, 01:20 UTC, respectively.

There was a huge dust event over northeast China on April 16, which traveled to the Sea of Japan on April 17. Probably due to the concentration of the dust and the

cloudless condition, it is easy to tell by looking at MODIS image (Figure 6 (a)) that dust is over the Sea of Japan since dust is brown while clouds are white. Both RGB1 and RGB2 images (Figure 6 (b) and (c), respectively) also show dust well, but with dark orange color and light green color, respectively.

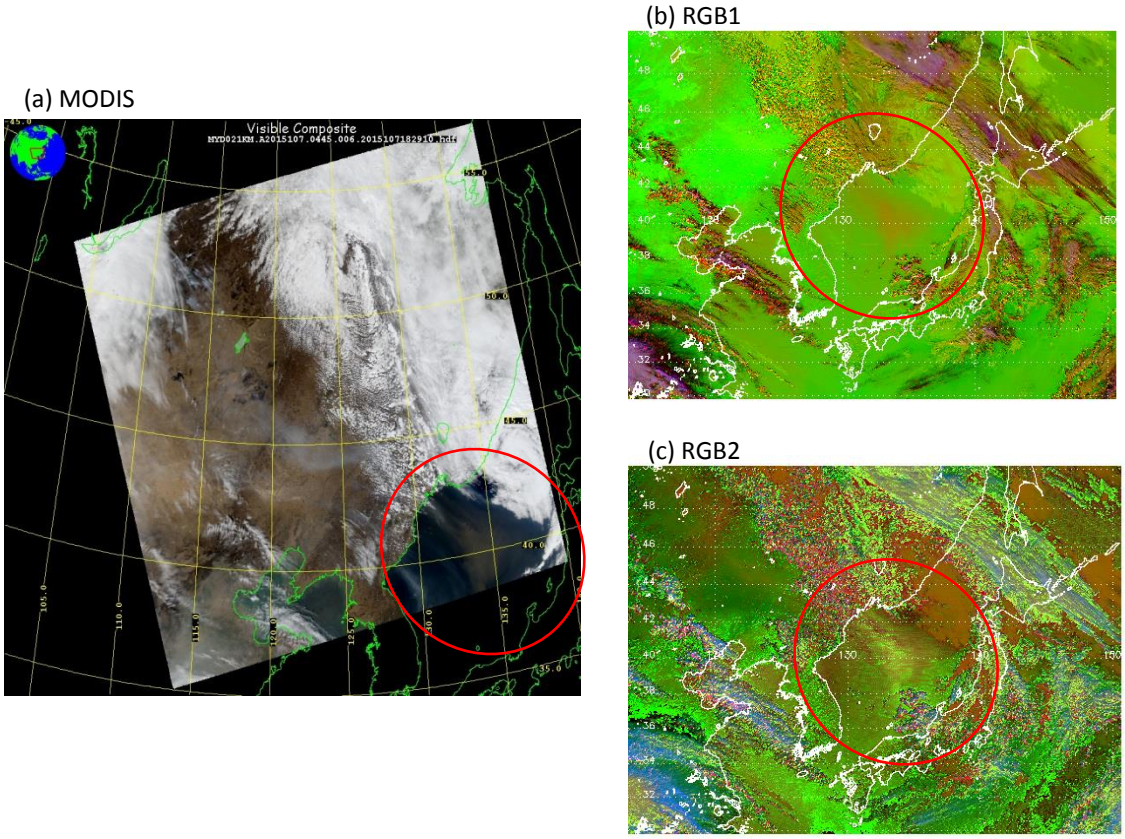

Figure 7 (a) MODIS image on 4/17/2015, 04:45 UTC. (b) and (c) RGB1 and RGB2 images on 4/17/2015, 04:40 UTC, respectively.

Images in Figure 7 are 3 hours and 20 minutes later than Figure 6. It can be seen that dust has moved over the Sea of Japan toward Japan, making this a good candidate for testing dust detection over the ocean.

4.2.3. April 27, 2015 case

(a) MODIS

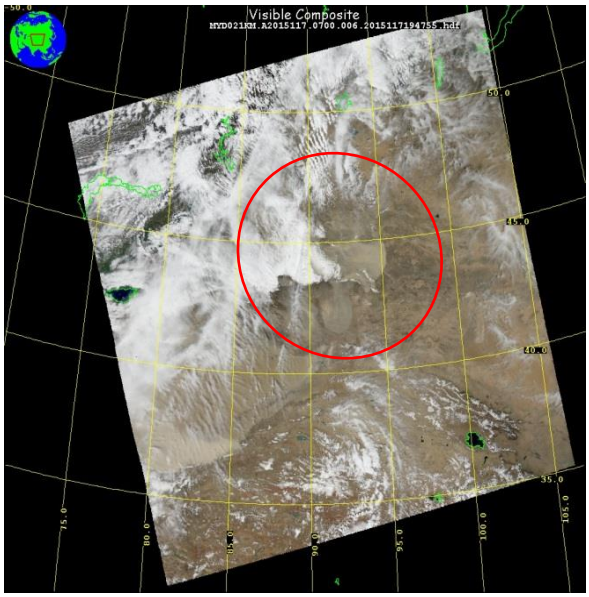

(b) RGB1

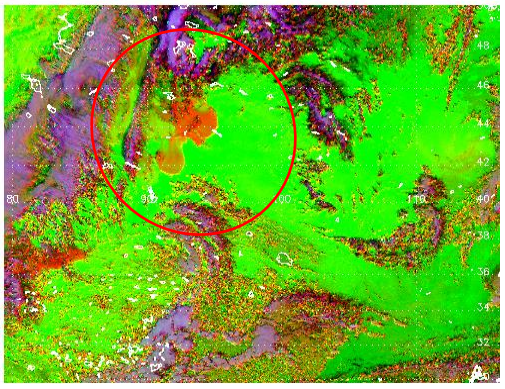

(c) RGB2

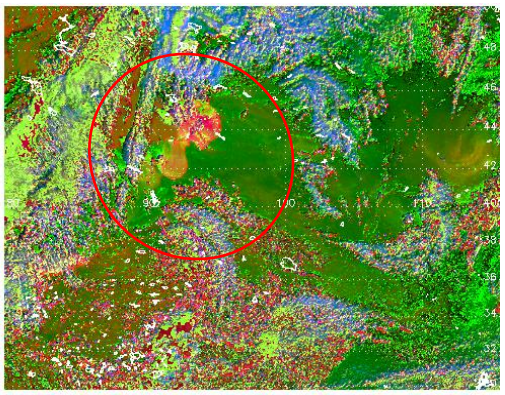

Figure 8 (a) MODIS image on 4/27/2015, 07:00 UTC. (b) and (c) RGB1 and RGB2 images on 4/27/2015, 07:00 UTC, respectively.

The dust event on April 27, 2015 happened over west part of Asia, and it seems likely that the event was huge, and dust spread widely. Since it happened inland, it takes a bit of time to identify dust by looking at MODIS image since the color of the dust is similar to the color of the surface (Figure 8 (a)); nevertheless, it is clear by looking at RGB1 and RGB2 images (Figure 8 (b) and (c), respectively). Comparing MODIS and RGB2 images, it seems likely that RGB2 displays dust as light green, pink, or dark pink. The fact that RGB2 sometimes displays dust as dark pink could make dust detection harder since land surface sometimes shows similar dark pink color on RGB2.

4.2.4. May 5, 2015 case

(a) MODIS

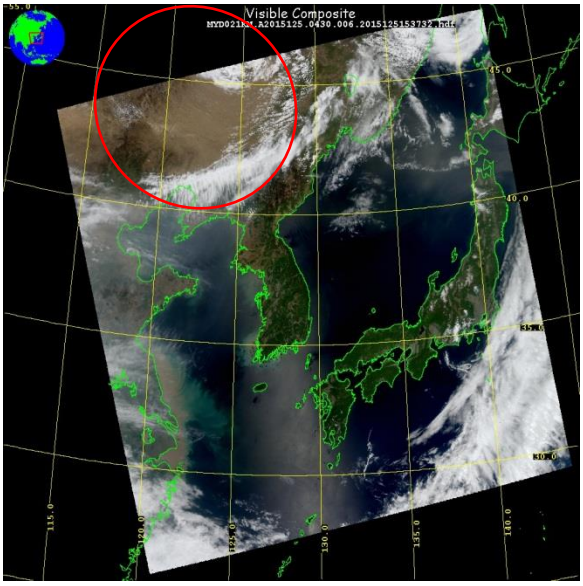

(b) RGB1

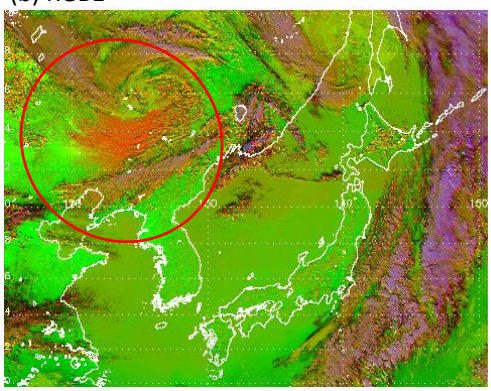

(c) RGB2

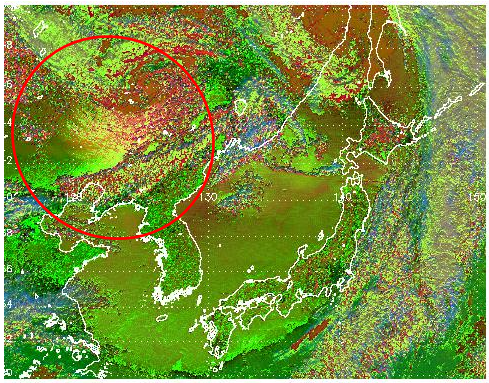

Figure 9 (a) MODIS image on 5/5/2015, 04:30 UTC. (b) and (c) RGB1 and RGB2 images on 5/5/2015, 04:30 UTC, respectively.

A dust event happened over the northeast of China on May 5, 2015. Since it happened over inland, it is not easy to tell where dust is by looking at the MODIS image alone (Figure 9 (a)); however, it is clear on the RGB1 image (Figure 9 (b)). It may seem noisy when looking at the RGB2 image (Figure 9 (c)). Other regions covered by clouds show light green color in the RGB2. This color is the same as dust's one, so if the new algorithm used RGB2 alone, it would detect these light green cloud regions as dust; however, the new algorithm first uses the color information in RGB1. These light green cloud regions in RGB2 have already been eliminated in the Base Step (see section 4.3.1)

where RGB1 is used, and the new algorithm can successfully define these regions as non-dust regions.

4.2.5. May 6 case

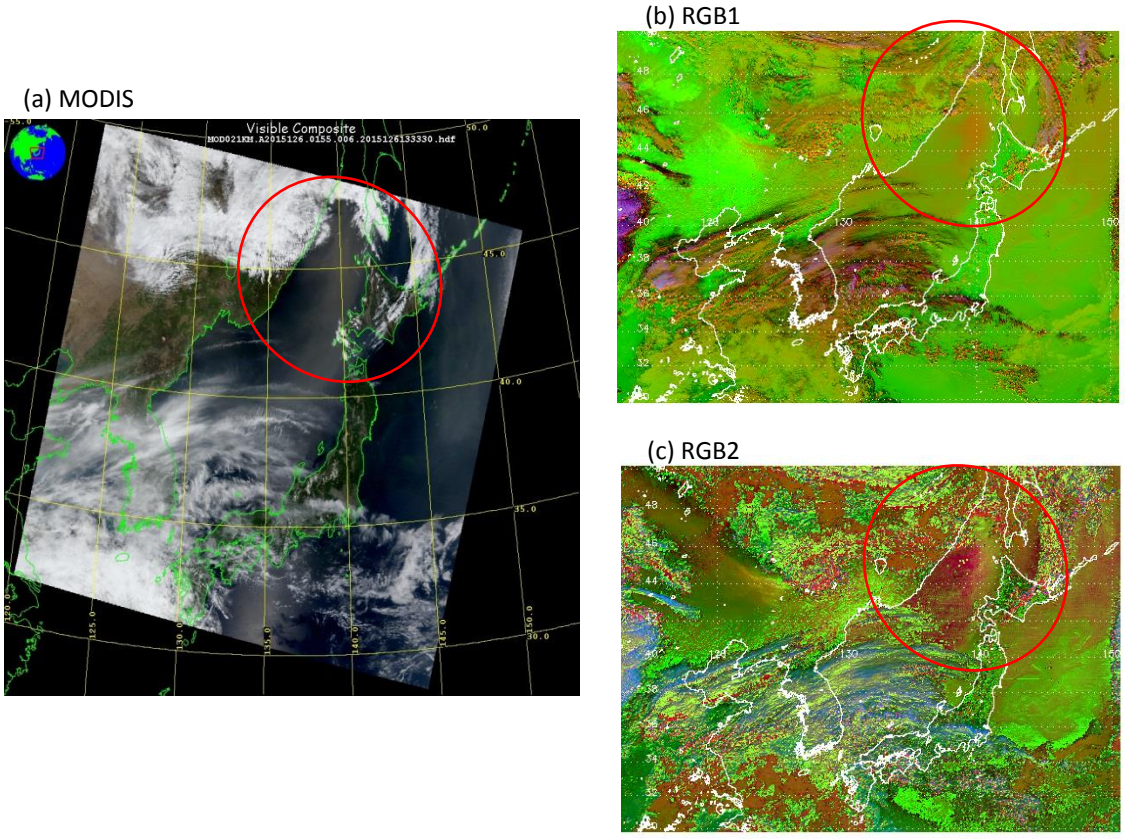

Figure 10 (a) MODIS image on 5/6/2015, 01:55 UTC. (b) and (c) RGB1 and RGB2 images on 5/6/2015, 01:50 UTC, respectively.

A dust event that happened on May 5 over northeast part of China traveled over the Sea of Japan on May 6. Even though the location of the dust was on the bright band in the MODIS image, it is still realizable in the MODIS image (Figure 10 (a)). It seems likely that the dust has become thin, and the color gets darker in the RGB1 (Figure 10 (b)) and the RGB2 (Figure 10 (c)).

4.3. Algorithm

The algorithm has been empirically developed based on the color information obtained from RGB1 and RGB2 composites. There are five steps to the algorithm: Base, Over Land, Over Sea, Possible Dust, and Smoothing. Table 7 is a flow chart summary of the algorithm. An elimination method is chosen for each step; in other words, all points are considered to be dust at the beginning and then non-dust area is eliminated step by step using the thresholds defined by color information derived from RGB1 and RGB2. The final step, Smoothing, also includes defining whether a region is dust or possible dust.

4.3.1. Base Step

Base Step is the fundamental step in the new algorithm. This step makes the new algorithm ready to eliminate false detection. Firstly, all points in the defined area, which is Asia in Table 3 in this study, are set to 1, which means dust. Secondly, if the brightness temperature at 11.2 μm channel is missing or invalid at some point, then it is set to 0 (non-dust). Thirdly, if the standard deviation of 11.2 μm channel is greater than 1 for a given pixel, then it is set as a non-dust pixel (0) to eliminate noises. Finally, the algorithm uses RGB1 data, and if $R1 < -0.5$, $G1 < -1.5$, $1 < G1$, or $B1 < 243$, then the pixel is set to non-dust (0). Here, R1, G1, and B1 are the ones introduced in Table 5. The RGB1 was chosen to be used in the Base Step since it shows dust relatively clearly. This allows most of the non-dust areas to be eliminated in the Base Step. The thresholds for RGB1, which are $R1 < -0.5$, $G1 < -1.5$, $1 < G1$, or $B1 < 243$, were empirically defined by converting RGB's color numbers (0 to 255 for each color) into the parameter's range for R1, G1, and B1, respectively.

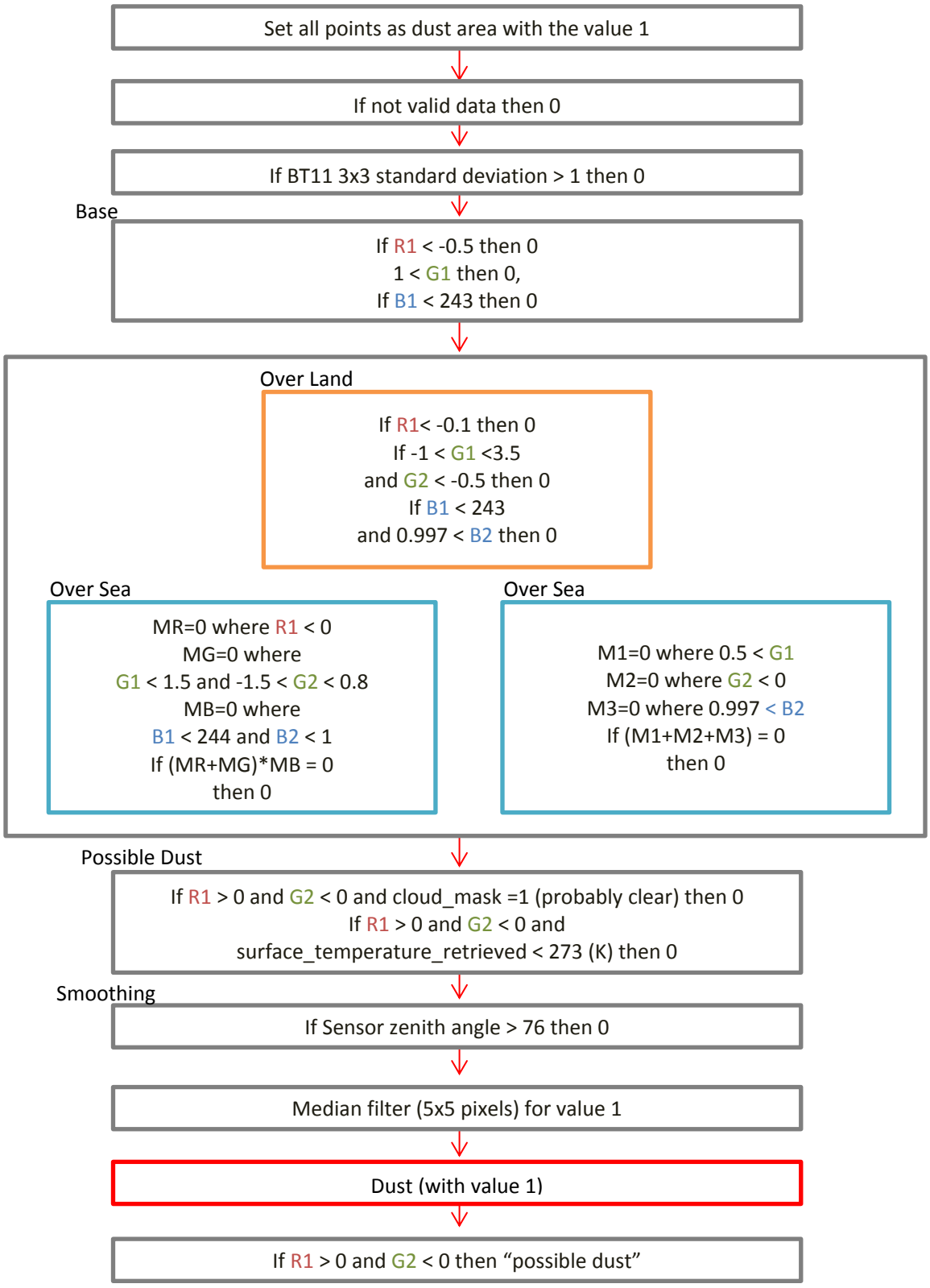

Table 7 The flow chart of the new dust detection algorithm

While the Base Step eliminates a majority of the non-dust areas, there are still some regions that are falsely marked as dust. The next three steps eliminate these incorrectly identified pixels using both RGB1 and RGB2 data.

4.3.2. Over Land

In the Over Land Step, the land surface that shows dust-like features is eliminated. In section 4.1.2, it was shown that dust is light green or pink over land, and the land surface is dark red in RGB2. Therefore, the dark red region will be eliminated on this step. The thresholds were empirically defined as follows: if $R1 < -0.1$, $-1 < G1 < 3.5$ and $G2 < -0.5$, or $B1 < 243$ and $0.997 < B2$ then the pixel is set 0.

Figure 11 (a) is the case on March 22 at 20 UTC, when there was no dust in the defined area in the midnight in local time. It is clear in the top left figure that the plumes falsely defined as dust show up sporadically over the continent in the Base Step. The top right figure, on the other hand, shows false dust detected in the Over Land step. There are still some plumes falsely detected as dust, but most of the plumes were eliminated. Figure 11 (b) is the case on April 16 at 20 UTC, at midnight local time. A dust event had occurred over northeast part of China, and it traveled to northeast coast of China. The top left figure shows dust defined in the Base Step. In addition to the dust plume over northeast coast of China, there are some plumes over the continent. This shows that the thresholds using the color information in RGB1 alone cannot eliminate the influence of land surface. On the other hand, the top right figure shows dust defined in the Over Land step. Although the area of the dust plume decreased a bit, the Over Land Step successfully eliminated most of the falsely detected dust; in other words, the dust-like land surface.

4.3.3. Over Sea

Here, the new three variables, MR, MG, MB, M1, M2, and M3 are introduced. Unlike the Over Land step, there are two steps for the Over Sea Step.

Step 1: After initializing MR, MG, and MB to 1, MR is set to 0 where R1 < 0, MG is set to 0 where G1 < 1.5 and -1.5 < G2 < 0.8, and MB is set to 0 where B1 < 243 and B2 < 1. If (MR + MG) x MB = 0 at some point then the pixel is set to 0, which means non-dust.

Step 2: After initializing M1, M2 and M3, M1 and M2 are set to 0 where 0.5 < G1 and G2 <0, respectively. M3 is set to 0 where 0.997 < B2. If (M1 + M2 + M3) = 0 then the pixel is set to 0.

These steps are implemented to eliminate the dark red color on RGB2 where RGB1 shows a dark orange color. Again, the dark orange color on RGB1 could be dispersed dust, land surfaces or sea with dust-like features. In RGB2, it shows light green color with less red for dispersed dust. When it comes to over oceans, the region which shows dust-like feature in RGB1 is mainly dark red in RGB2; hence, it is possible to remove non-dust regions on this step.

Figure 11 (c) shows the case on April 27 at 10 UTC, when a huge dust event happened over northwest part of China. The top left figure shows dust defined in the Over Land Step, and the dust-like land surface has been eliminated already. There was no dust over the Sea of Japan on April 27; however, there is a plume falsely defined as dust on the top left figure. The top right figure shows dust defined in the Over Sea Step. There are still small plumes falsely defined as dust over the Sea of Japan; nevertheless, the Over Sea Step

successfully eliminates falsely detected dust in the Base Step, making it possible that IR channels alone can distinguish dust over ocean.

4.3.4. Possible Dust

False detection happens mostly during nighttime over land, especially when the surface temperature is less than 273 (K) (see Section 5.3). To eliminate this low surface temperature influence, pixels are set to 0 if R1 > 0 and G2 < 0 and cloud mask is defined as "probably clear." Besides, pixels are set to 0 if R1 > 0 and G2 < 0 and the surface temperature derived from surface temperature retrieved by CLAVR-x is less than 273 (K). The threshold "R1 >0 and G2 <0" means that a pixel could be "possible dust," and this will be explained in the next section.

Figure 12 (a) shows the case on March 22 at 20 UTC, where there was no dust in the defined region. After the Over Sea Step, the new algorithm still shows some false detection (Figure 12 (a) top left); however, after the Possible Dust Step, most of the false detection was eliminated (Figure 12 (a) top right). Figure 12 (b) is the case on April 27 at 19 UTC. After the Over Sea Step, there are false detection plumes at the top middle and its right (Figure 12 (b) top left). On the other hand, these plumes were mostly eliminated by the Possible Dust Step as you can see in the image in the top right of Figure 12 (b). It is worth noting that the actual dust plumes over west part of China are successfully detected in Figure 12 (b), and was not eliminated by the Possible Dust Step. Figure 12 (c) is the case at 22 UTC on March 5, 2016. There is a huge dust plume over northeast part of China. After the Over Sea Step, there are false detection plumes at the bottom of the top left figure; however, the amount of the plumes decreased drastically after the Possible Dust Step

(Figure 12 (c) top). In this case, cloud mask data was not available, and surface temperature retrieved data alone was used in the Possible Dust Step.

Hence, combining three information that are "possible dust," "probably clear," and "the surface temperature," which are derived from the new algorithm, the cloud mask of CLAVR-x, and the surface temperature retrieved on CLAVR-x, respectively, it is possible to eliminate most of the false detection. Once again, the false detection is further explained in the section 5.3.

4.3.5. Smoothing

There are two steps for the Smoothing Step. First, noises are eliminated at the peripheral of the observing range. Any pixels with a sensor zenith angle greater than 76^{o} are set to non-dust (0). Second, a 5 x 5 pixel median filter is applied to smooth and eliminate noise from the data. Here, 5 x 5 pixel median filter was chosen because 3 x 3 pixel median filter is too narrow for the smoothing, and 10 x 10 pixel median filter smooths too much.

As shown in Section 4.1.2, dust in RGB2 is light green as well as pink. As the dust disperses, the pink color becomes darker and becomes harder to distinguish from the land. Because of this, it was decided that light green color in RGB2 is considered as "dust" and pink or dark pink color is considered as "possible dust". This allows the new algorithm to define "possible dust" for regions that might be falsely detected dust. For this reason, the RGB2 threshold for "possible dust" is set as follows: $0 < R2$ and $G2 < 0$.

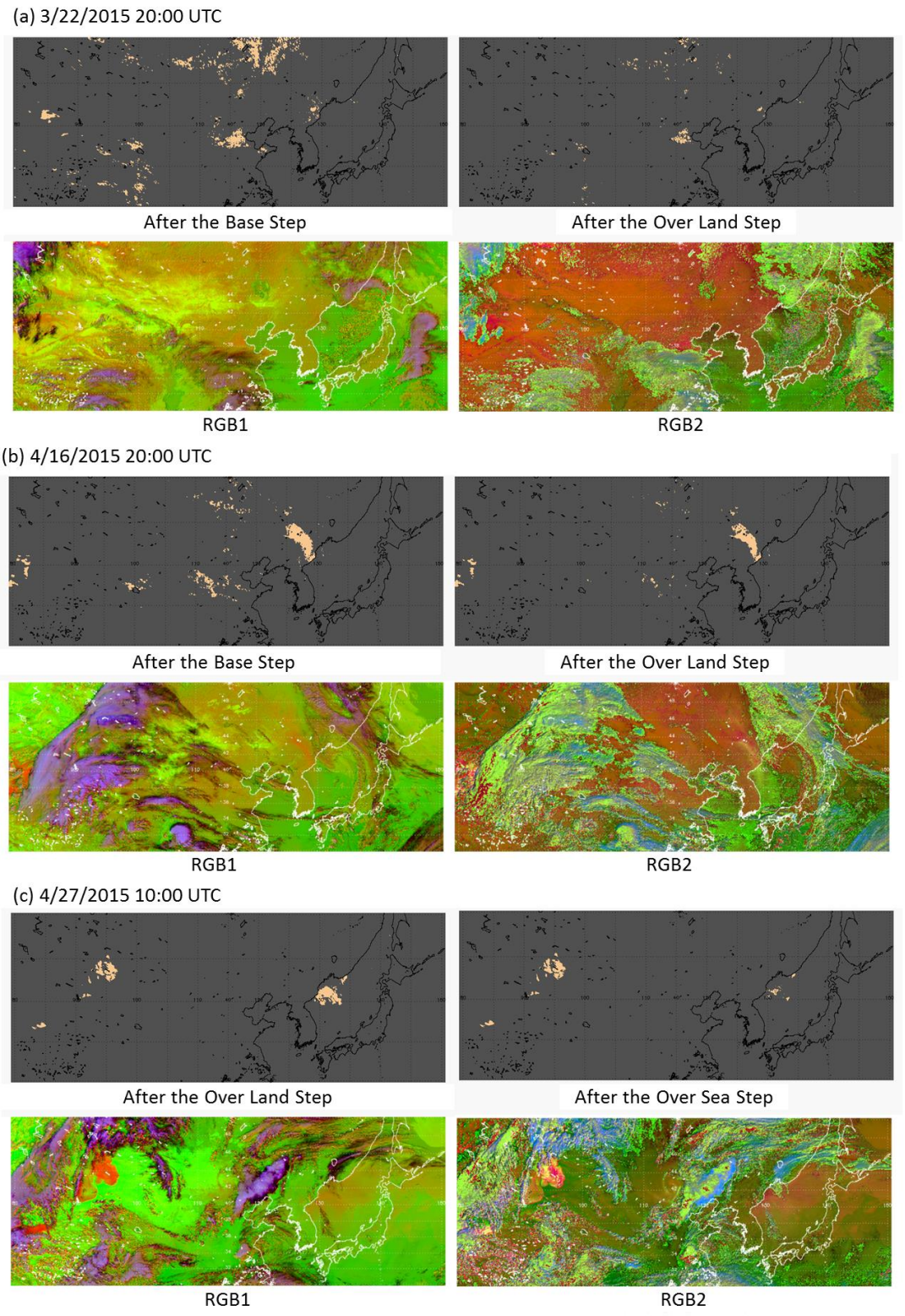

Figure 11 (a) Dust defined in the Base Step (top left) and in the Over Land Step (top right) on March 22, 2015 at 20 UTC, (b) dust defined in the Base Step (top left) and in the Over Land Step (top right) on April 16, 2015 at 20 UTC, and (c) dust defined in the Over Land Step (top left) and in the Over Sea Step (top right) on April 27, 2015 at 10 UTC. All with corresponding RGB1 and RGB2 at the bottom.

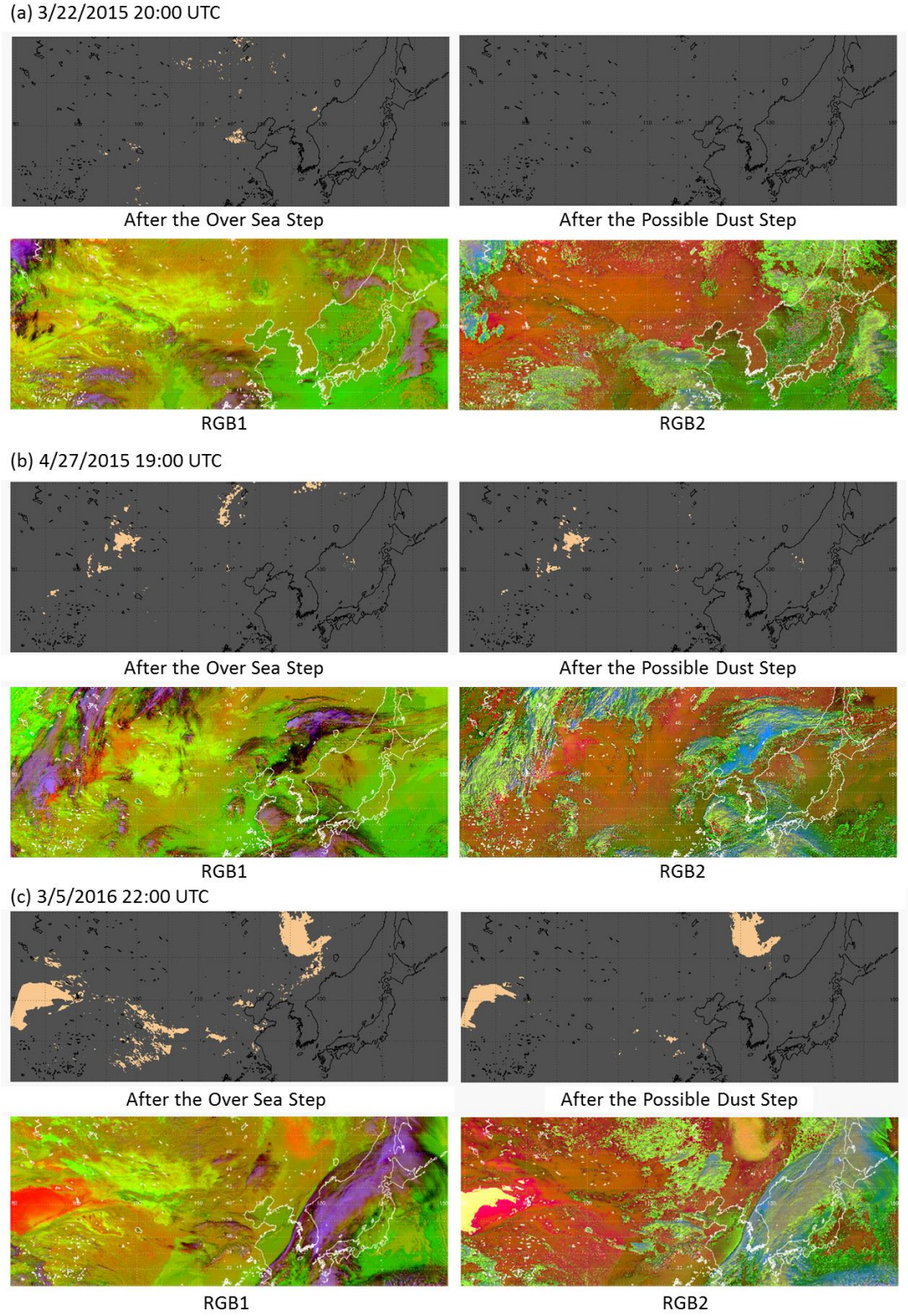

Figure 12 (a) Dust defined in the Over Sea Step (top left) and in the Possible Dust Step (top right) on March 22, 2015 at 20 UTC, (b) dust defined in the Over Sea Step (top left) and in the Possible Dust Step (top right) on April 27, 2015 at 19 UTC, and (c) dust defined in the Over Sea Step (top left) and in the Possible Dust Step (top right) on March 5, 2016 at 22 UTC. All with corresponding RGB1 and RGB2 at the bottom.

5. Results

This section will be discussing the results of the new algorithm, which was introduced in section 4, as applied to the selected test cases. The results of the new algorithm will be compared with the results of the algorithm in Zhang et al. (2006). For simplicity, the algorithm developed by Zhang et al. (2006) is hereafter called "the algorithm 2006." As previously discussed, the algorithm in Zhang et al. (2006) cannot detect dust over oceans.

5.1. During daytime

5.1.1. April 16 at 10:00 UTC

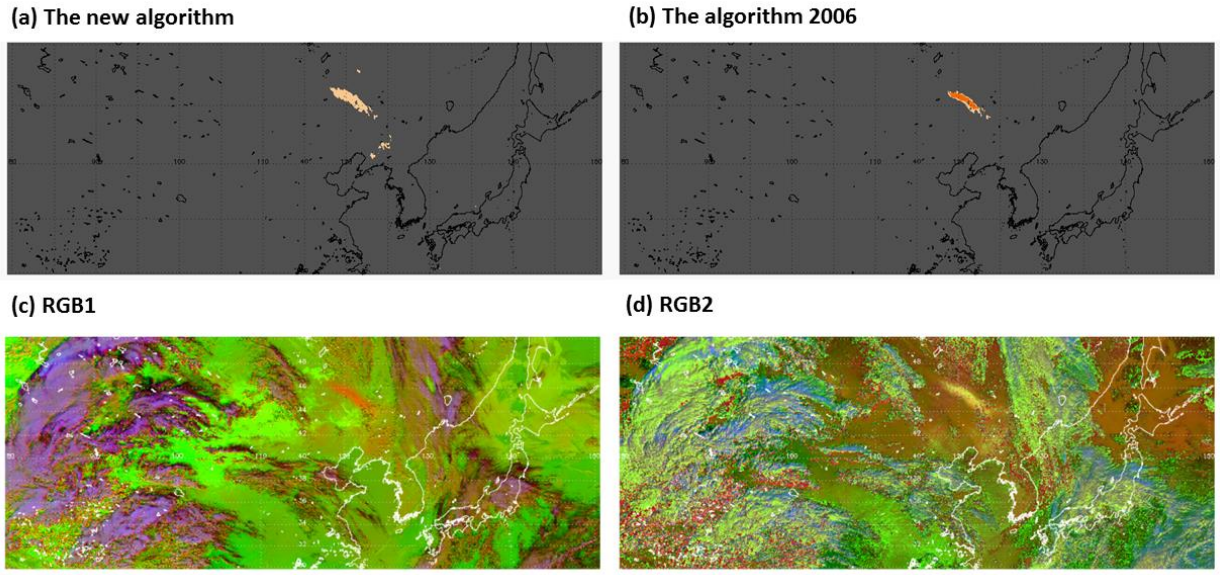

Figure 13 (a) Dust index calculated by the new algorithm in section 4. White: dust, orange: possible dust. (b) Dust index calculated by the algorithm in Zhang (2006). White: relatively weak dust, orange: relatively strong dust. (c) RGB1, (d) RGB2. All on April 16 at 10:00 UTC.

Figure 13 (c) and (d) show dust over northeast part of China on April 16 at 10:00 UTC. Dust detected using the new algorithm and in the Zhang et al. (2006) are shown in Figure 13 (a) and (b), respectively. While both algorithms properly detected dust, the area

of dust in the new algorithm is a little bit larger. One notable difference between the two algorithms is that the algorithm 2006 shows the strength of the dust. While this could be applied to the new algorithm, the main focus is on detecting dust and distinguishing dust from falsely detected dust.

The new algorithm shows some plumes over north side of Korean Peninsula, and since these plumes do not move when watching the animation of the April 16 case, the plumes could be falsely detected as dust. The reason why the new algorithm picked these plumes as dust is due to the color information of the plumes in RGB1 and RGB2. The new algorithm defines the region as dust when it shows orange (R1 is positive and G1 is slightly positive) to dark orange (R1 is slightly positive and G1 is around 0 (K) or slightly negative) color in RGB1, and light green or pink in RGB2. The plumes show dark orange in RGB1 and light green in RGB2 even though it is hard to tell by human eyes.

5.1.2. April 17 at 4:00 UTC

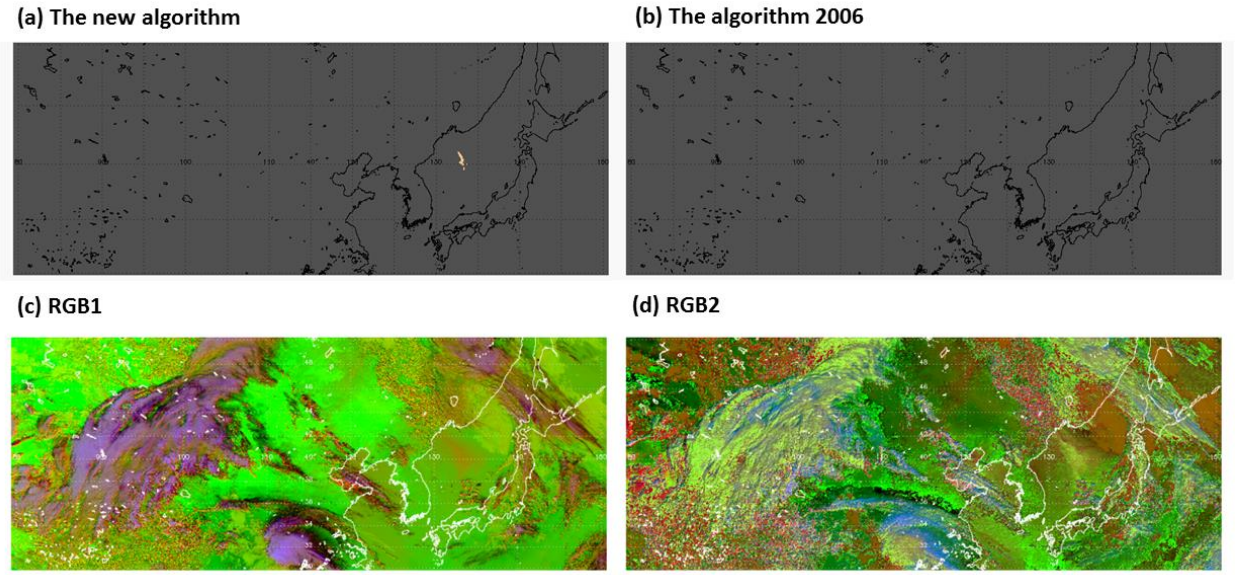

Figure 14 Same as Figure 13 but on April 17 at 4:00 UTC.

At 4 UTC on April 17, dust that had occurred over northeast part of China traveled over the Sea of Japan and has been dispersed. It is hard to tell where dust is by looking at the still images of RGB1 and RGB2 (Figure 14 (c) and (d), respectively); however, the animations of RGB1 and RGB2 show that there was a dust plume over the Sea of Japan. Since dust has been dispersed, it is dark orange in RGB1 (Figure 14 (c)) and less light green in RGB2 (Figure 14 (d)). Figure 14 (a) shows dust detected in the new algorithm, and there is small plume of dust over the Sea of Japan. The algorithm 2006 does not show any dust over the Sea of Japan since it does not catch dust over oceans. Even though the area of dust is small in the new algorithm when compared to the areas of dust in RGB1 and RGB2, it proves that the new algorithm can detect dust not only over land but over the ocean as well. The algorithm 2006 uses 8.5 μm, 11 μm and 12 μm channels alone, and similar channels

are used in RGB1; hence, using RGB1 alone cannot detect dust over oceans. It is safe to say that RGB2 plays an important role in detecting dust over the ocean.

5.1.3. April 27 at 10:00 UTC

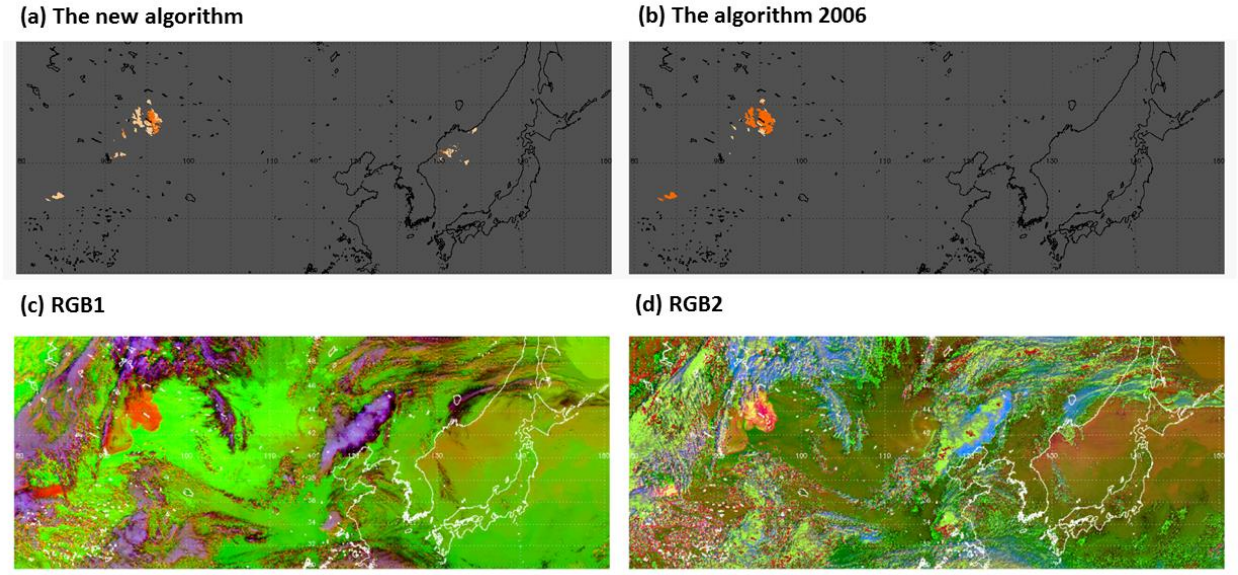

Figure 15 Same as Figure 13 but on April 27 at 10:00 UTC.

There was a huge dust event generated over northwest part of China on April 27, and it can easily be seen by looking at the still images of RGB1 and RGB2 (Figure 15 (c) and (d), respectively). Dust is vivid orange (R1 is positive and G1 is slightly negative) in RGB1, and it is pink, dark pink or light green in RGB2. There are three dust plumes; the north, the middle, and the south. The new algorithm captured all three plumes even though the middle's area is small (Figure 15 (a)), while the algorithm 2006 detected the north and the south plumes and not the middle (Figure 15 (b)). It can be said that the new algorithm is more sensitive to dust in this case. When taking a look at the Sea of Japan, the new algorithm shows the false detection due to the dust-like feature over there in RGB1 and RGB2. As explained in section 4.3.3, the effect of this dust-like feature was mostly

eliminated by the color information derived from RGB2. However, if the non-dust region shows dust-like feature in RGB2, it is hard to completely eliminate the false detection.

5.1.4. May 5 at 9:00 UTC

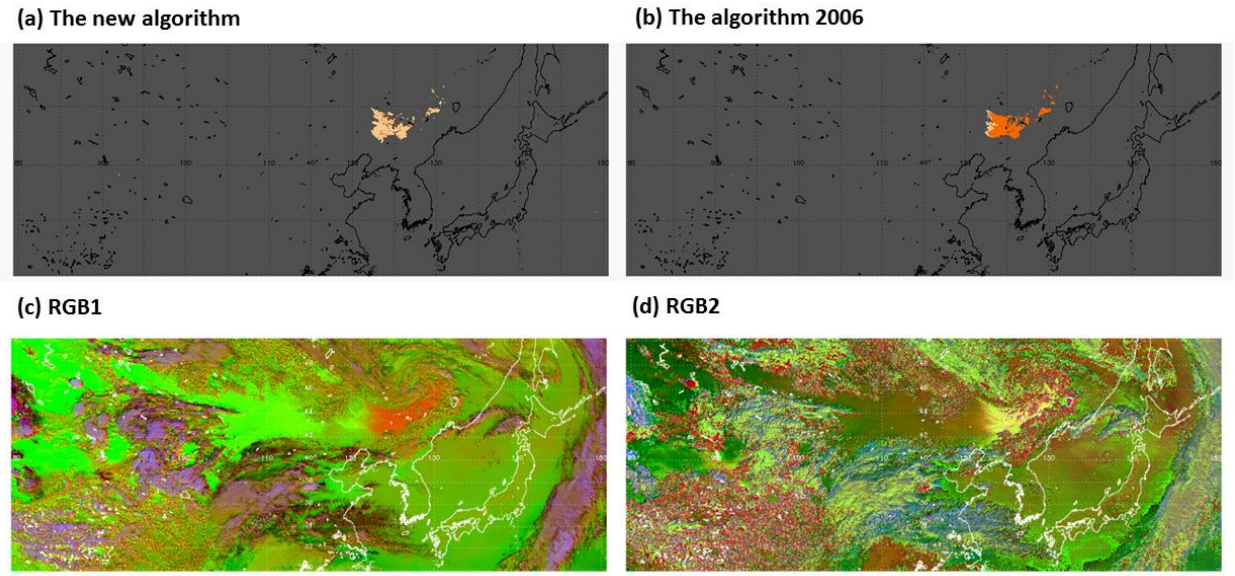

Figure 16 Same as Figure 13 but on May 5 at 9:00 UTC.

Dust had generated over northeast part of China and it traveled to the Sea of Japan from May 5 to 6. Dust is displayed as a large orange plume in RGB1 and a light green plume in RGB2 (Figure 16 (c) and (d), respectively). Both the new algorithm and the algorithm 2006 detected dust well in this case (Figure 16 (a) and (b), respectively).

5.1.5. May 6 at 0:00 UTC

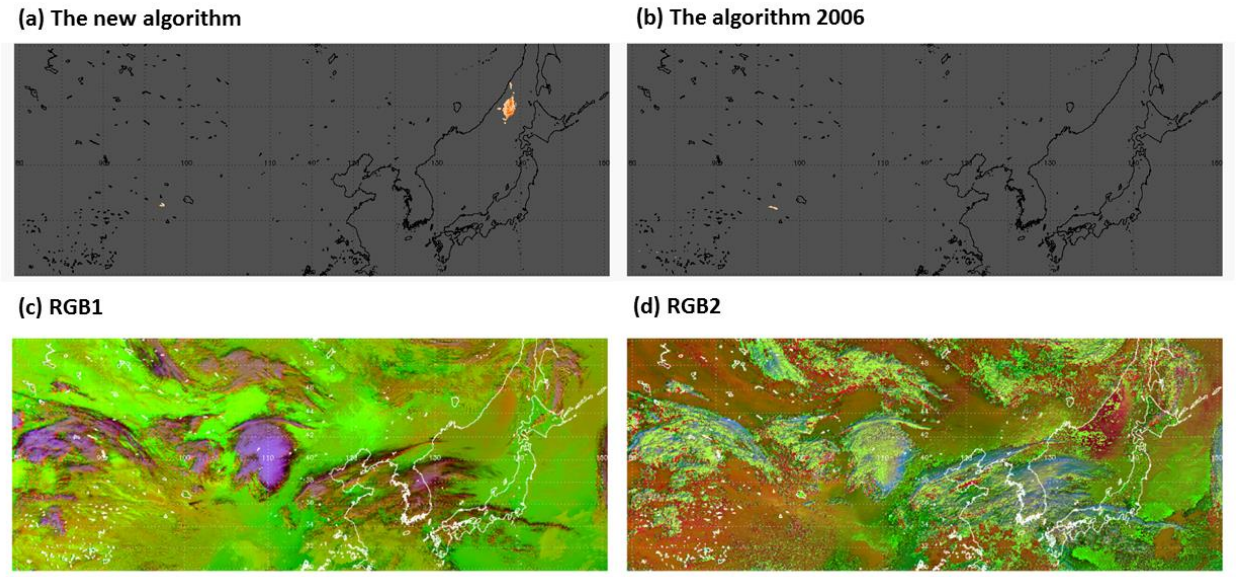

Figure 17 Same as Figure 13 but on May 6 at 00:00 UTC.

As the dust that had been generated on May 5 traveled to the Sea of Japan, it gradually lost the vividness in its color both in RGB1 and RGB2 (Figure 17 (c) and (d), respectively), and its color got closer to the color over the dustless Sea of Japan. Still, it is possible for the new algorithm to identify dust as it can be seen in Figure 17 (a). Since the algorithm 2006 does not capture dust over the ocean as shown in Hong (2009), the result of the algorithm 2006 (Figure 17 (b)) does not show any dust over the Sea of Japan.

There is a small spot detected as dust over the continent in the left side of both images of the new algorithm and the 2006 algorithm. Both algorithms work quite well during daytime; however, the algorithms cannot completely eliminate the false detection.

5.2. During the nighttime

5.2.1. March 22 at 0:00 UTC

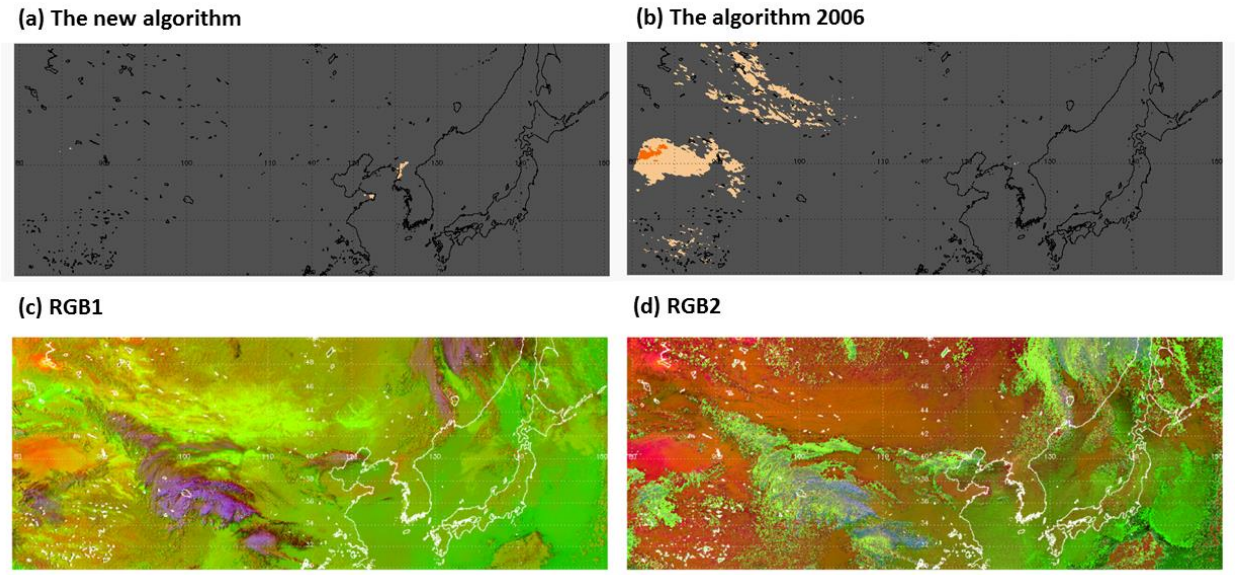

Figure 18 Same as Figure 13 but on March 22 at 0:00 UTC.

In the case of March 22 at 0:00 UTC, dust is not obvious in the still images of RGB1 and RGB2 (Figure 18 (c) and (d), respectively); nevertheless, when checking the animations of RGB1 and RGB2 images, it was confirmed that there was dust around Korean Peninsula. The new algorithm (Figure 18 (a)) successfully captured dust over Korean Peninsula, while the algorithm 2006 did not (Figure 18 (b)). Remember that the channels used in drawing RGB1 are similar to the ones used in the algorithm 2006. When it comes to eliminating the false detection over dust-like land surface, using RGB2 in addition to RGB1 allows the new algorithm to capture dust, which the algorithm 2006 cannot. While the algorithm 2006 falsely detected dust over the Taklamakan Desert, the new algorithm successfully eliminated the false detection there. As explained in section 4.3.4, the dust-like land surface is eliminated by using the color information derived from RGB2. Again, RGB2 plays an important role in decreasing the amount of false detection.

It should be noted that the new algorithm had had false detection over the Taklamakan Desert after the Over Sea Step (section 4.3.3). However, the false detection over there was eliminated by the following Possible Dust Step (section 4.3.4). The falsely detected dust over the Taklamakan Desert mostly appeared during nighttime, and it was assumed that the cause of the false detection could be the temperature drop over the land surface. This temperature drop issue will be discussed at the end of this chapter (section 5.3). It also has to be noted that the new algorithm failed to detect dust over the East Sea even though it was shown that the new algorithm is sensible to dust over the ocean in previous sections. In this March 22 case, the color of the dust over the East Sea in RGB1 is a little too dark, and the threshold defined for RGB1 in the Base Step eliminated most of the part of dust over the sea; hence, if dust is dispersed, it is difficult to detect it.

5.2.2. April 16 at 21:30 UTC

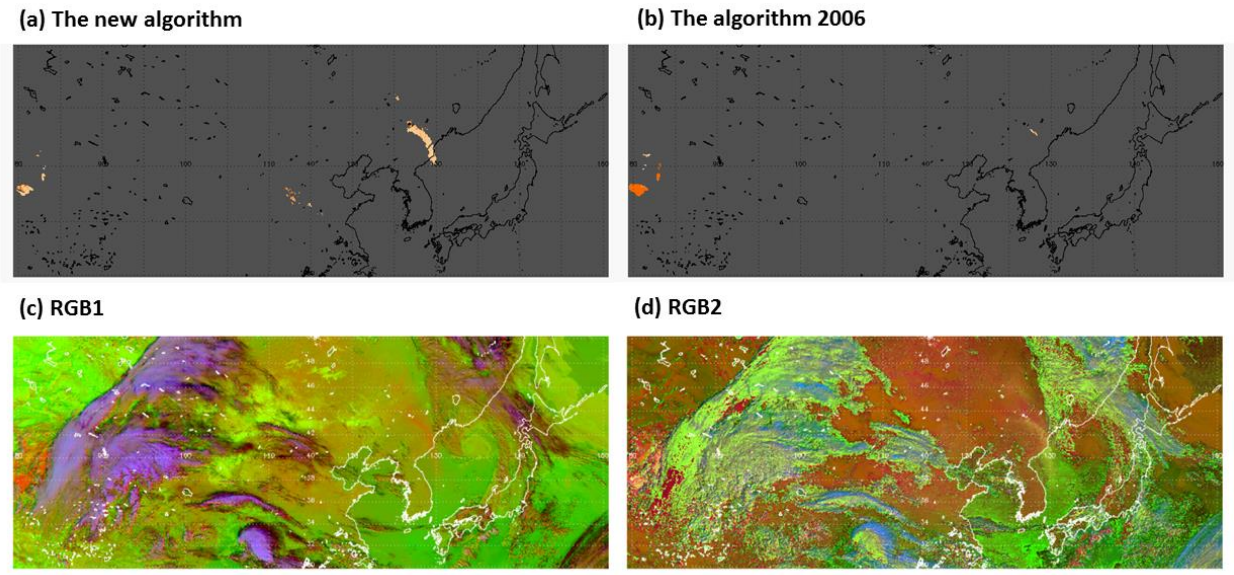

Figure 19 Same as Figure 13 but on April 16 at 21:30 UTC.

Dust that had been generated in northeast part of China on April 16 traveled over to the Sea of Japan around 21:30 UTC as it can be seen on the RGB1 and RGB2 images (Figure 19 (c) and (d)). The new algorithm could successfully and smoothly detect dust over land and the Sea of Japan (Figure 19 (a)) while the algorithm 2006 underestimated the area of dust plume over land (Figure 19 (b)). Since the algorithm 2006 is not for detecting dust over the ocean, it does not show any dust over the Sea of Japan.

There are some small spots over southeast part of China in the new algorithm. Since the color is orange, it was defined as "possible dust." Since those plumes do not move when looking at the animation, the plumes would be falsely detected dust. Both the new algorithm and the algorithm 2006 detected a small dust plume over the Taklamakan Desert. Since there were mostly covered by clouds, it is hard to tell even by looking at the animation whether it is dust or falsely detected dust. It is necessary to keep in mind that, if

there are thick clouds, it is hard to detect dust because dust could be under the clouds or it is well mixed with the clouds.

5.2.3. April 17 at 15:00 UTC

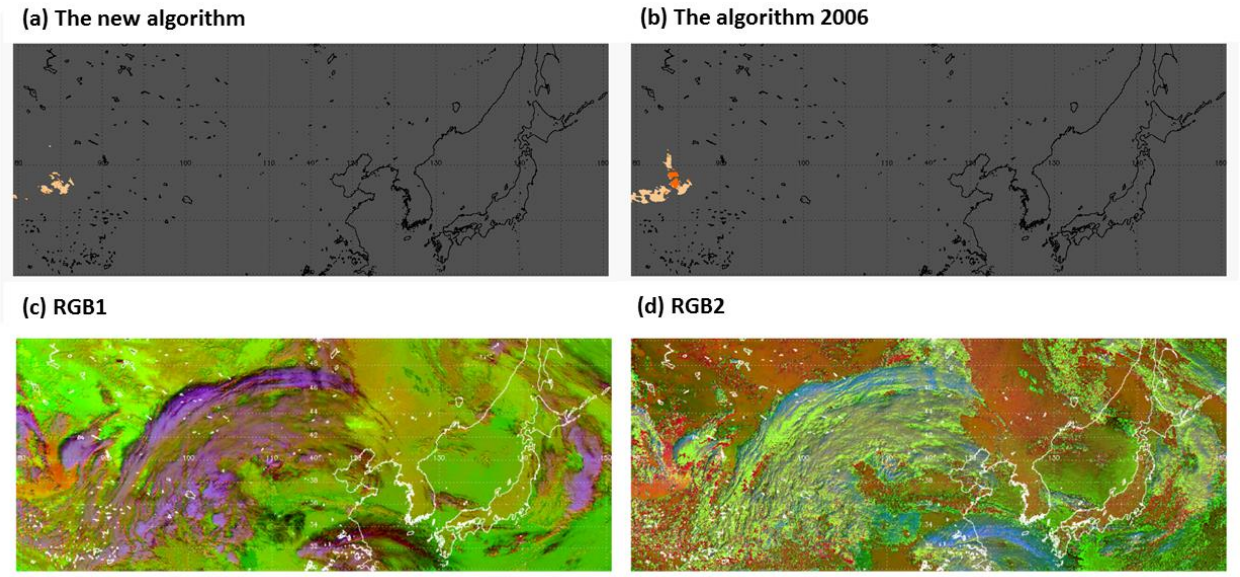

Figure 20 Same as Figure 13 but on April 17 at 15:00 UTC.

As dust traveled over to the Sea of Japan, it got more difficult to identify dust in both RGB1 and RGB2. When looking at these animations, it was shown that dust reached for the west coast of Japan around 12:00 UTC. At 15:00 UTC, there was no dust that can be identified with human eyes in RGB1 or RGB2 (Figure 20 (c) and (d), respectively). Considering that the new algorithm underestimated the area of dust over the Sea of Japan in section 5.1.2, it had been easy to perceive that the new algorithm would not be able to capture dust as much as our eyes can do. In fact, the detection done by the new algorithm failed to capture dust after 9:00 UTC on April 17.

At 15:00 UTC, both the new algorithm and the algorithm 2006 detected dust over the Taklamakan Desert (Figure 20 (a) and (b), respectively). Again, since there were

thick clouds over the desert, it is hard to tell whether the detected plumes are dust or not even by watching the animation of RGB1 and RGB2.

5.2.4. April 27 at 19:00 UTC

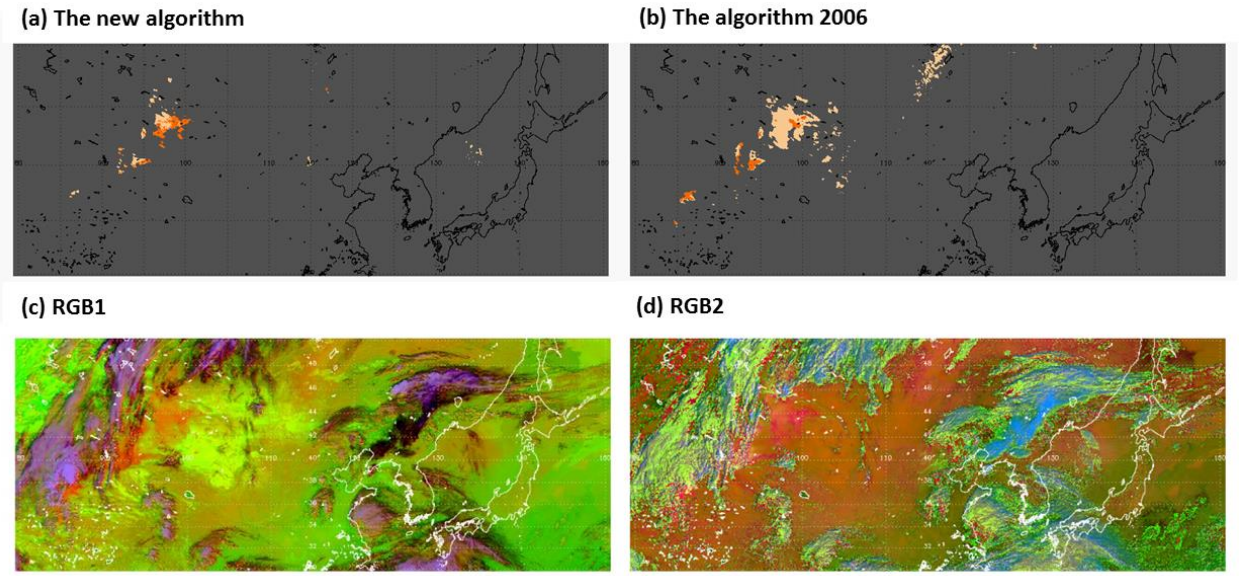

Figure 21 Same as Figure 13 but on April 27 at 19:00 UTC.

A huge dust event over northwest part of China happened on April 27 as introduced in section 5.1.3. Dust plumes had spread over land and it lasted during nighttime as well. The new algorithm slightly underestimated the area of dust, which was called “the north” in section 5.1.3, when comparing to the algorithm 2006 (Figure 21 (a) and (b), respectively), yet both algorithms captured dust quite well.

False detection appeared over east Mongolia in the 2006 algorithm while the new algorithm successfully eliminated false detection by the Possible Dust Step (section 4.3.4). It has been assumed that the false detection was caused by the drop of the surface temperature during the nighttime. In fact, when looking at Figure 21 (c) and (d), east

Mongolia regions in both RGB1 and RGB2 show similar colors as dust plumes such as dark orange and dark pink, respectively. This will be discussed further in section 5.3.

5.2.5. April 27 at 23:00 UTC

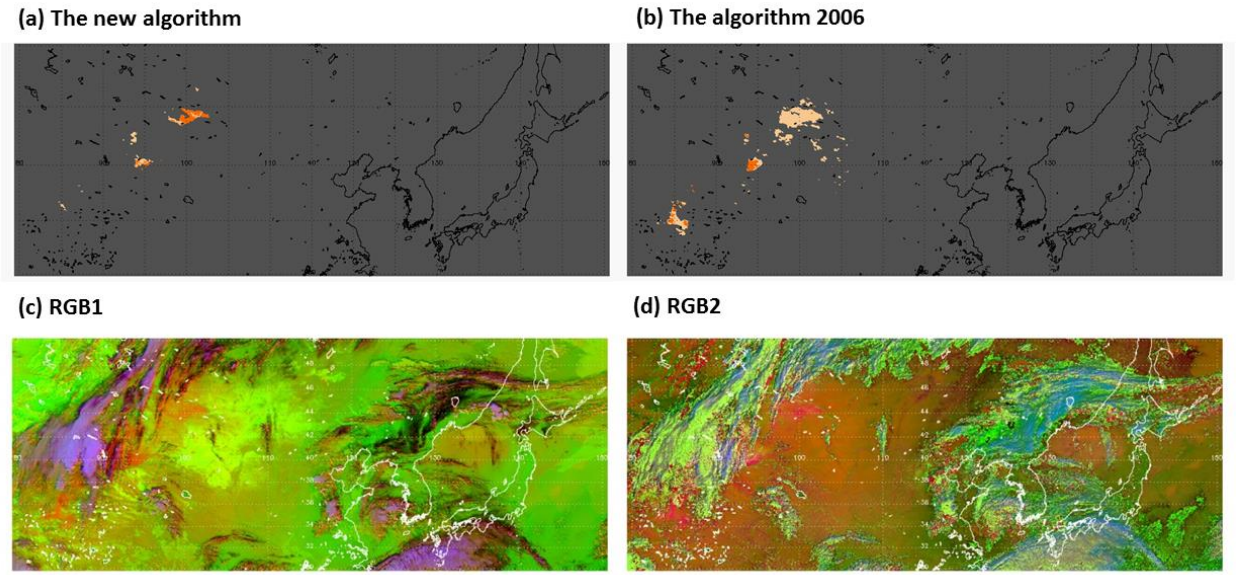

Figure 22 Same as Figure 13 but on April 27 at 23:00 UTC.

As the morning came, the false detection over east Mongolia shown in section 5.2.4 disappeared in the algorithm 2006 (Figure 22 (b)). When looking at the RGB1 and RGB2 images (Figure 22 (c) and (d), respectively), it can be seen that the color of the region that was falsely detected as dust in 5.2.4 lost orange feature in RGB1 and pink color in RGB2; in other words, it could be interpreted that the land surface lost its dust-like features when the morning came.

5.2.6. May 5 at 18:00 UTC

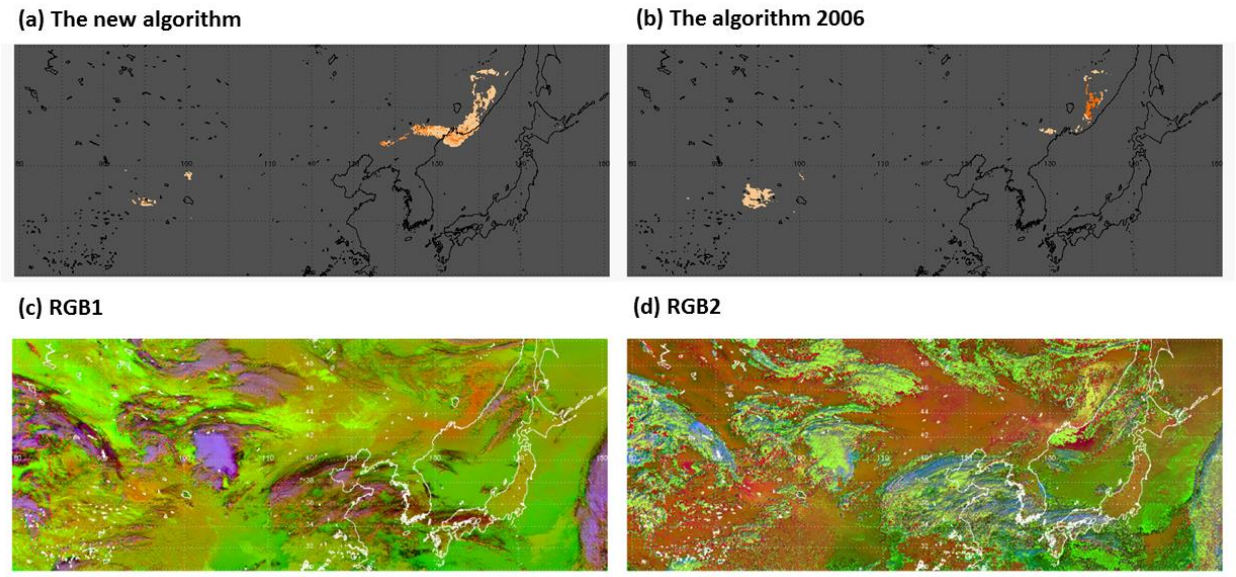

Figure 23 Same as Figure 13 but on May 5 at 18:00 UTC.

Dust that had been generated over northeast part of China traveled over to north part of the Sea of Japan on May 5. Figure 23 (a) shows that the new algorithm detected dust smoothly over land and sea. The algorithm 2006 (Figure 23 (b)), on the other hand, underestimated the area of dust and did not detect dust over the sea. It can be said that, if there is no cloud, the new algorithm can detect dust quite well even dust is straddled over land and the ocean.

Both algorithms, however, falsely detected dust over central China. This could also be due to the drop in the surface temperature during nighttime.

5.2.7. June 9 at 14:00 UTC

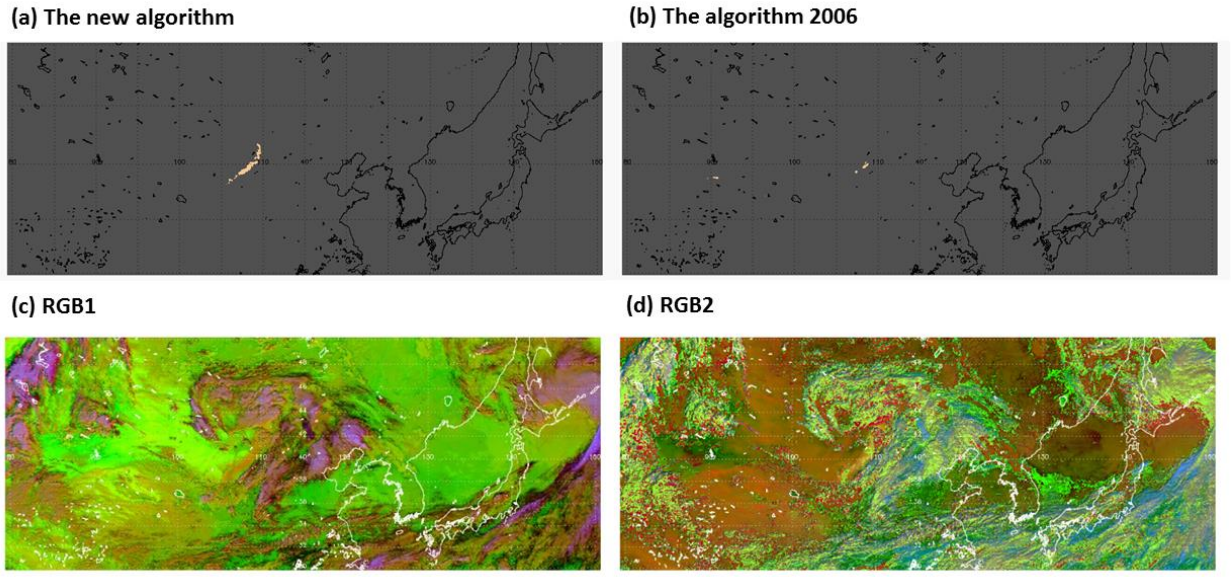

Figure 24 Same as Figure 12 but on June 9 at 18:00 UTC.

Figure 24 shows a dust event happened over Gobi Desert on June 9. Since there were clouds over the desert, it is hard to confirm dust by looking at RGB1 and RGB2 (Figure 24 (c) and (d), respectively). Both the new algorithm and the algorithm 2006 had successfully detected dust; however, as time went and dust got dispersed, the algorithm 2006 could not capture dust (Figure 24 (b)) while the new algorithm did (Figure 24 (a)). It seems likely that the new algorithm is more sensitive in detecting dust when compared to the algorithm 2006, and it can monitor dust longer period of time.

5.3. False detection

Before coming up with the idea of introducing the Possible Dust Step (section 4.3.4), the new algorithm had had difficulty distinguishing dust from dustless regions during nighttime. It was assumed that the false detection would be highly related to the change in the clear sky surface temperature. It should be noted that, in this section, the results of the new algorithms are the ones that were done without using the Possible Dust Step. The reason for not using the Possible Dust Step in this section is to explain the effect of the surface temperature drop.

Figure 25 shows the comparison between the early night and midnight on April 27, 2015. As it can be seen, the image at 14:00 UTC (Figure 25 (a-1)) does not show any dust in north part of China. However, at 19:00UTC, (Figure 25 (b-1)) dust is detected over the region. When animating this case, the "dust" detected at 19:00 UTC stayed stationary. Thus, it was assumed that these were falsely detected dust. The 11 μm brightness temperature (BT) for both 14:00 UTC and 19:00 UTC (Figure 25 (a-2) and (b-2), respectively) are also shown, and these display that this region had no cloud present. The surface temperature can be retrieved by using the atmospherically corrected 11 μm radiance. The derived surface temperature shows that the temperature decreased from 14:00 UTC (Figure 25 (a-3)) to 19:00 UTC (Figure 25 (b-3) from >273K to <273K. This decrease in surface temperature could lead the region look like dust in RGB1 and RGB2 (Figure 25 (b-4) and (b-5), respectively). In RGB1, the region, which was falsely detected as dust, tends to be orange more brightly when compared to other dustless regions and the region at 14:00 UTC (Figure 25 (a-4)). In RGB2, it seems that the region shows more pink

color when compared to the region at 14:00 UTC (Figure 25 (a-5)). Therefore, the new algorithm without going through the Possible Dust Step (section 4.3.4) tends to define a non-dust region as dust when the surface temperature drops during nighttime, in other words, when the region shows dust-like feature in both RGB1 and RGB2. In fact, the false detection increases during nighttime or relatively colder days such as in winter. When the Possible Dust Step (section 4.3.4) is used, the false detection in Figure 25 (b-1) disappears as can be seen in section 5.2.4.

Figure 26 images are the case on March 5, 2016. The images on the left are at 8:30 UTC and on the right are at 22:00 UTC. The plumes over northeast part of China are dust, and these can be identified by looking at RGB1 and RGB2 (Figure 26 (a-4) and (b-4) for 8:30 UTC, and (a-5) and (b-5) for 22:00 UTC, respectively). Even at 8:30 UTC, which is the daytime in local time, the new algorithm defines part of the Taklamakan Desert as dust (Figure 26 (a-1)). The region is cloudless in Figure 26 (a-2), and the surface temperature over there shows less than 270 K in Figure 26 (a-3). When looking at Figure 26 (b-1), which is the image at 22:00 UTC, the new algorithm shows orange colored dust plumes over the southern part of China in addition to the region over the Taklamakan Desert. When looking at the animation of this day, these plumes stay there during nighttime. The region is cloudless according to Figure 26 (b-2), and the temperature is less than 273 K when looking at Figure 26 (b-3). Again, when the Possible Dust Step (section 4.3.4) is used, the false detection in Figure 26 (b-1) decreases significantly as can be seen in Figure 12 (c).

Figure 27 shows the case in June, when the temperature is obviously higher than in March. Images on the left are the ones at 8:30 UTC on June 10, 2016 and images on the right are at 22:00 UTC on the same day. The new algorithm did not detect any dust at 8:30

UTC. The Taklamakan Desert was covered by clouds at both 8:30 UTC and 22:00 UTC (Figure 27 (a-2) and (b-2), respectively), but south part of China was relatively clear at both times. When looking at south part of China, the surface temperature is more than 273 K in at 22:00 UTC (Figure 27 (b-3)), and the new algorithm did not detect dust.

When considering that the new algorithm showed dust on March 5, 2015 during nighttime over south part of China as introduced in the third paragraph in this section, the surface temperature would be one of the factors that causes the false detection in the new algorithm; hence, the Possible Dust Step (section 4.3.4) was introduced in the new algorithm to eliminate the effect of the surface temperature drop.

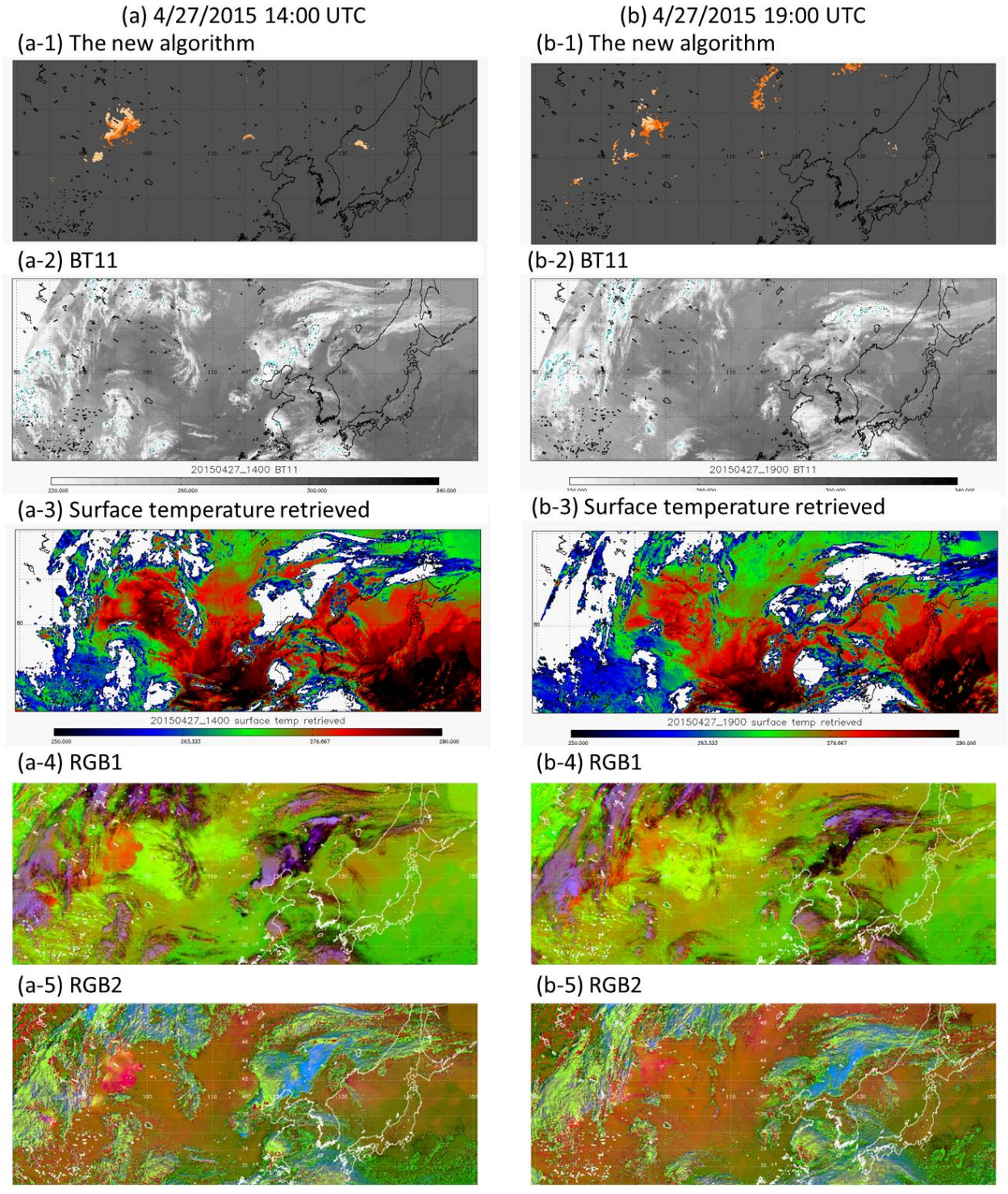

Figure 25 Comparison of results between 14:00 UTC and 19:00 on April 27, 2015 for (a) dust detected by the new algorithm. White: dust, orange: possible dust. (b) Brightness temperature at 11 μm. (c) Surface temperature retrieved. (d) RGB1. (e) RBG2. It should be noted that (a-1) and (b-1) did not go through the Possible Dust Step (section 4.3.4).

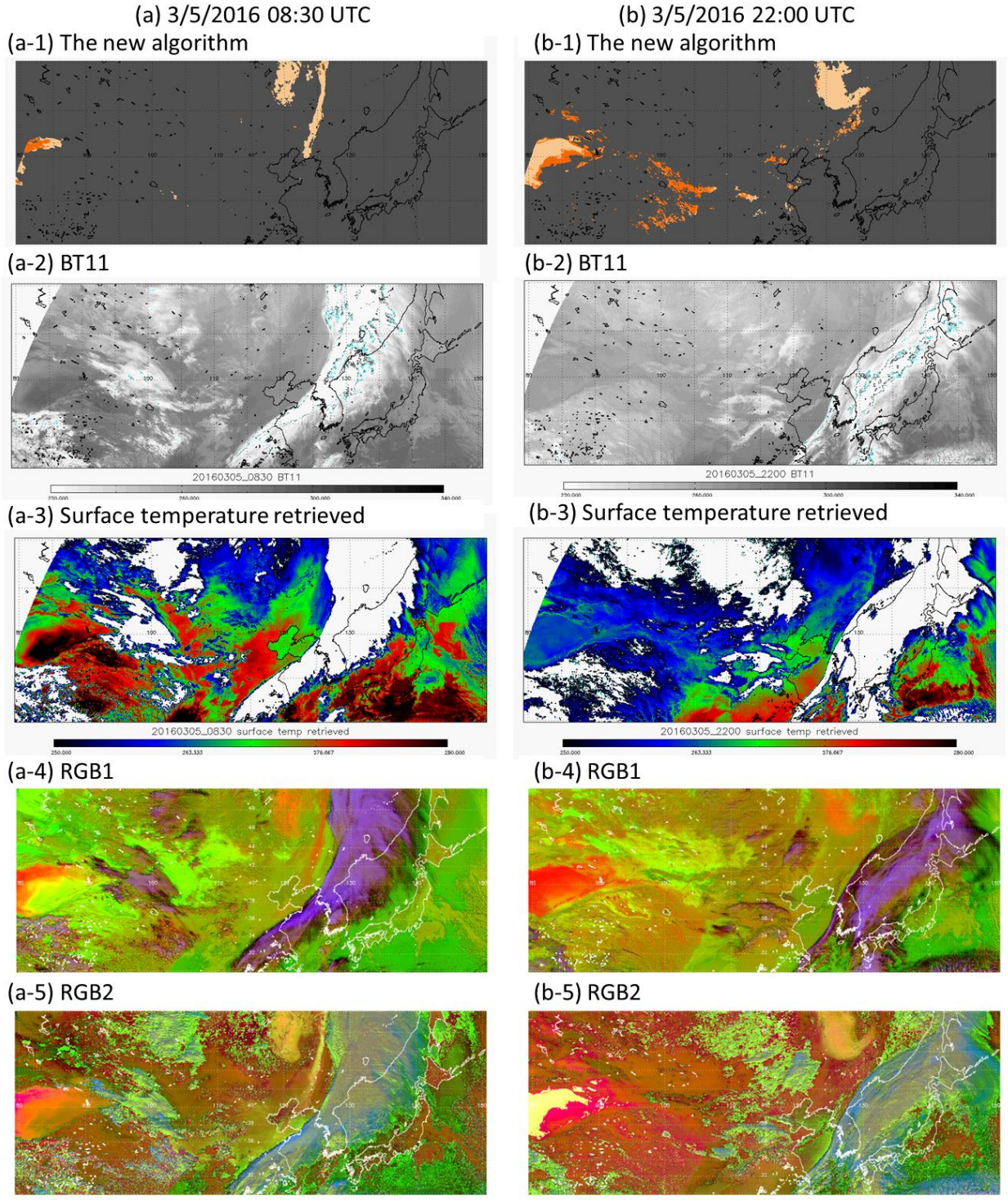

Figure 26 Same as Figure 24 but on March 5, 2016 at 08:30 UTC and 22:00 UTC.

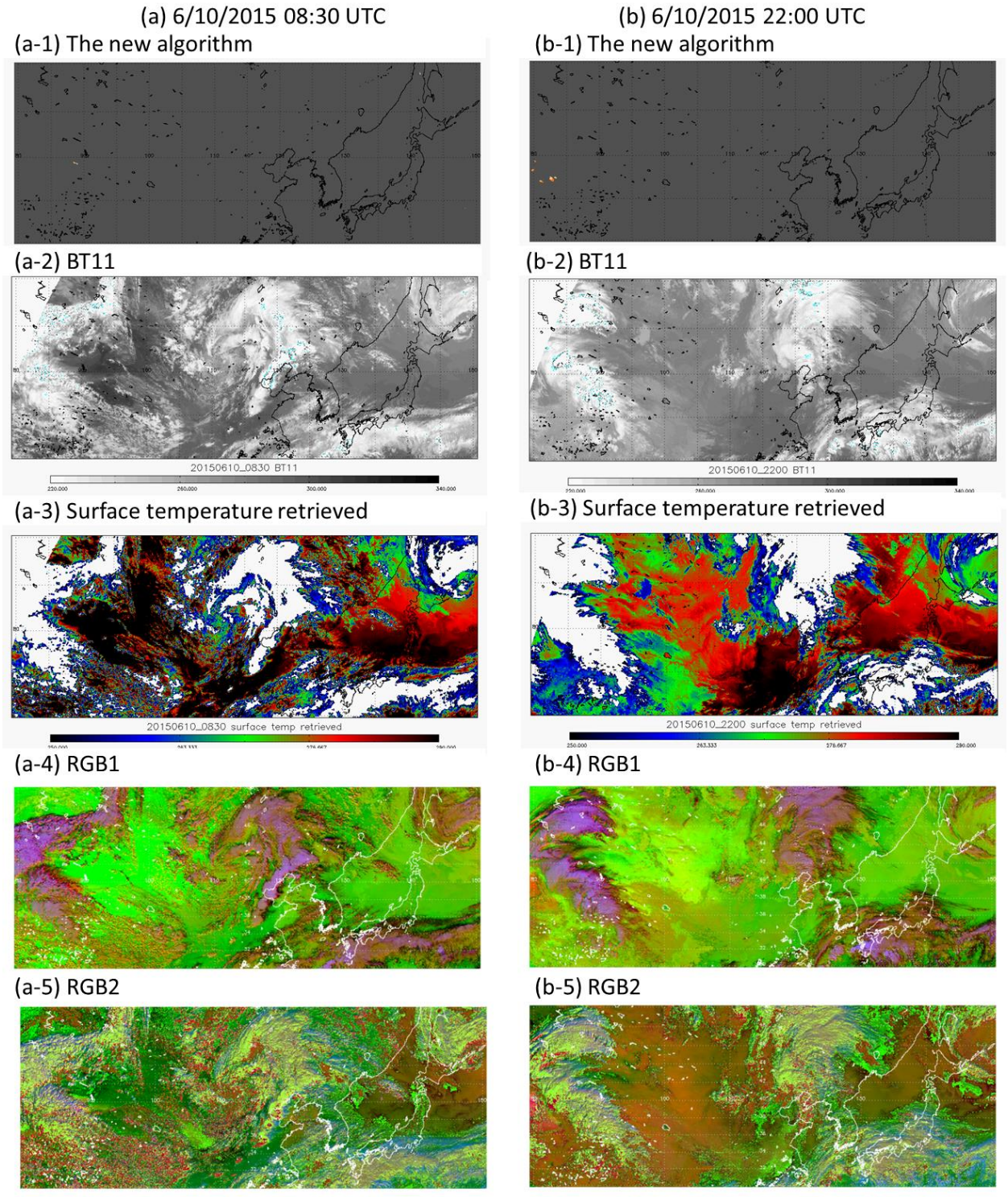

Figure 27 Same as Figure 24 but on June 10, 2015 at 08:30 UTC and 22:00 UTC

6. Conclusions

A new algorithm for dust detection was developed using brightness temperatures of four infra-red channels: 8.6 μm, 10.4 μm, 11.2 μm, and 12.4 μm, which are available on the Advanced Himawari Imager (AHI), carried by JMA's Himawari-8 geostationary meteorological satellite. Previous research has shown that IR channels alone can detect dust over land, but suffered difficulties over the ocean. It has also been known that using visible channels as well as near IR channels increases the accuracy of dust detection during the daytime. However, the near IR and visible channels depend on the sunlight to identify features, making them ineffective for dust detection at night. There are IR channels carried by AHI that, while similar to the ones used in previous research, have slight differences in the wavelength compared to previous instruments. It is expected that the differences in the IR channels on AHI could make it possible to detect dust over the ocean as well as over land.

The new algorithm was developed based on the information derived from two RGB images called RGB1 and RGB2. Both RGBs use only IR channels, which mean they can be used both during the day and night. Thresholds for the two RGBs were introduced in Table 5 and Table 6, respectively. Dust is expressed with orange in RGB1, and light green or pink in RGB2. The reason why dust in RGB1 is orange is because R1, the brightness temperature between 12.4 μm and 11.2 μm, shows positive value in aerosol regions and G1, the brightness temperature difference between 11.2 μm and 8.6 μm, is slightly negative in aerosol regions (see section 4.1). The physics behind BGB2 should be investigated to explain why RGB2 captures dust properly. Based on these color information, thresholds are

defined as in the flow chart introduced in Table 7. During daytime, the algorithm presented detects dust quite well over both land and the ocean, making it possible to monitor dust in the observing range of AHI. The algorithm can also detect dust during nighttime. There are some limitations at night, however. In particular, it occasionally falsely defines cold, cloudless surface regions as "dust." It is possible that one of the reasons why the new algorithm considers these regions as dust is that the cold surface temperature during nighttime that shows similar features as dust does. This was more noticeable in the winter months than summer, when the surface temperature is colder. The false detection due to the surface temperature drop is mostly eliminated by the Possible Dust Step (section 4.3.4); however, not all false detection can be removed. It is safe to say that if the dust event happens during warm season, the new algorithm would have less false detection over land than in the cold season.

When compared with the results of an algorithm introduced by Zhang et al (2006), which uses three channels 8.6 μm, 11.2 μm, and 12.4 μm, the new algorithm can reduce the amount of falsely detected dust over the cloudless regions. For example, the new algorithm is more sensitive to relatively thin dust as in the cases of March 22 (section 5.2.1), and did not underestimate the area of dust as the Zhang et al (2006) algorithm did in the cases of April 16 and 17, May 5 and 6, and June 9 2015. Because the channels used for RGB1 are similar ones that are used for the algorithm 2006, it is safe to assume that the information derived from RGB2 is what helps to identify non-dust area without eliminating or underestimating dust. In particular, the two window channels, 10.4 μm and 11.2 μm, could be the key in the new algorithm when it comes to the sensitiveness to dust. In addition, the new algorithm can detect dust over the ocean while the Zhang et al (2006)

algorithm does not. It can be said that the most important achievement of the study is that the new algorithm displays smooth transfer of dust from land to the ocean regardless of time slots: daytime or nighttime.

One issue with the new algorithm is that it cannot detect widely dispersed dust. There were several examples where JMA reported dispersed dust over Japan while the algorithm did not detect any dust. Using IR channels alone could be one of the reasons why it is impossible to detect widely dispersed dust with the new algorithm. This assumption is consistent with the findings of Cho et al. (2013). They stated that the algorithms using simple brightness temperature difference, D-parameter method (Roskovensky and Liou, 2005), and the multichannel image may be more effective for thick dust detection rather than thin dust detection.

While all the cases presented were during the post-launch test period for AHI (prior to July 2015), it is expected that the thresholds for the dust algorithm will not change. However, there are areas of further improvement which can be explored in the future. So far, the biggest problem in detecting dust happens during nighttime due to the false detection over cloudless or relatively cloudless regions that show dust-like features, especially in the cold season. It is assumed that this is due to cold land surface pixels of clear pixels. This could be an effect of the usage of the 11 μm channel or using only IR channels. As the quality of cloud mask product improves, it could be more helpful to determine clear/cloudy pixels.

Overall, even though it sometimes detects the land surface with dust-like feature as dust during nighttime and it cannot detect very thin dust, the new algorithm can monitor dust all day and both over land and the ocean. While the physics behind RGB1 can be

explained by previous research, it is needed to investigate the spectral emission signatures for RGB2 to explain the physics behind it and why this algorithm works very well. However, it would be nice if the algorithm developed in this study can be of help for daily operations in the countries that have had dust issues every year.

7. References

Ackerman, S. A., 1989: Using the Radiative Temperature Difference at 3.7 and 11 μm to Track Dust Outbreaks, *Remote Sens. Environ.,* **27**, 129-133.

Ackerman, S. A. and K. I. Strabala, 1994: Satellite remote sensing of H_2SO_4 aerosol using the 8- to 12 μm window region: Application to Mount Pinatubo, *Journal of Geophysical Research*, **Vol. 99, NO. D9**, 18639-18649.

Ackerman, S. A., 1997: Remote sensing aerosols using satellite infrared observations, *Journal of Geophysical Research,* **Vol. 102, NO. D14**, 17069-17079.

Ahn, M., Min, J., Chung, C., Nam, J., 2003: Effects of the tropospheric dust on the sea surface temperature derivation from the GMS-5 IR data, *Journal of Korean Meteorological Society*, **39**, 653–666.

Cho, H. M., S. L. Nasiri, and P. Yang, 2013: Detection of Optically Thin Mineral Dust Aerosol Layers over the Ocean Using MODIS, *Journal of Atmospheric and Oceanic Technology*, **30**, 896-916.

Ellrod, G. P., B. H. Connell, D. W. Hillger, 2003: Improved detection of airborne volcanic ash using multispectral infrared satellite data. *Journal of Geophysical Research,* **Vol. 108, NO. D12**, AAC 6-1 – AAC 6-13.

Fraser, R. S., 1976: Satellite measurement of mass of Sahara dust in the atmosphere. *Applied Optics*, **Vol. 15 No.10**, 2471-2479.

Hashimoto, T., and N. Ohkawara, 2007: Development of "Kosa monitoring Product" from infrared data of the geostationary meteorological satellite (MTSAT-1R). *Meteorological Satellite Center Technical Note,* **49**, March, 1-17.

Hao, X., and J. J. Qu, 2007: Saharan dust storm detection using moderate resolution imaging spectroradiometer thermal infrared bands, *Journal of Applied Remote Sensing,* **1**, 1-9.

Heidinger, A., A. Walther, D. Botambekov, W. Straka III, and S. Wanzong, 2014: The Clouds from AVHRR Extended User's Guide Version 5.4.1, *NOAA*.

Hong, S., 2009: Detection of Asian dust (Hwangsa) over the Yellow Sea by decomposition of unpolarized infrared reflectivity, *Atmospheric Environment,* **43**, 5887-5893.

Iwasaka Y., H. Minoura, and K. Nagaya, 1983: The transport and special scale of Asian dust-storm clouds: a case study of the dust-storm event of April 1979. *Tellus,* **35B**, 189-196.

Kaufman, Y. J., A. E. Wald, L. A. Remer, B. C. Gao, R. R. Li, and L. Flynn, 1997: The MODIS 2.1-μm Channel – Correlation with Visible Reflectance for Use in Remote Sensing of Aerosol. *IEEE Transactions on Geoscience and Remote Sensing,* **Vol. 35, No.5**, 1286-1297.

Kim, K. W., Y. J. Kim, and S. J. Oh, 2001: Visibility impairment during Yellow Sand periods in the urban atmosphere of Kwangju, Korea. *Atmospheric Environment,* **35**, 5157-5167.

Kim, K. H., G. H. Choi, C.H. Kang, J. H. Lee, J. Y. Kim, Y. H. Youn, and S. R. Lee, 2002: The chemical composition of fine and coarse particles in relation with the Asian Dust events. *Atmospheric Environment,* **37**, 753-765.

Kwon, H. J., S. H. Cho, Y. Chun, F. Lagarde, and G. Pershagen, 2002: Effects of the Asian Dust Events on Daily Mortality in Seoul, Korea. *Environmental Research Section,* **90,** 1-5.

Lin, T. H., 2001: Long-range transport of yellow sand to Taiwan in Spring 2000: observed evidence and simulation. *Atmospheric Environment,* **35,** 5873-5882.

Martínez, M. A., J. Ruiz, and E. Cuevas, 2009: Use of SEVIRI images and derived products in a WMO Sand and Dust Storm Warning System. *IOP Publishing, IOP Conference Series: Earth and Environmental Science 7 (2009)*, 012004.

McClain, E.P., Pichel, W.G., Walton, C.C., 1985: Comparative performance of AVHRR based multichannel sea surface temperature, *Journal of Geophysical Research*, **90**, 11587–11601.

Meteorological Satellite Center of Japan Meteorological Agency, 2015: Dust RGB, Detection of Yellow Sand (Asian Dust), *website*.

Meteorological Satellite Center of Japan Meteorological Agency: Himawari-8/9, Imager (AHI), *website*.

Mori, I., M. Nishikawa, T. Tanimura, and H. Quan, 2003: Change in size distribution and chemical composition of kosa (Asian dust) aerosol during long-range transport. *Atmospheric Environment,* **37**, 4253-4263.

NASA MODIS: Specifications, *website*.

Prata, A.J., 1989: Observations of volcanic ash clouds in the10–12 mm window using AVHRR/2 data, *International Journal of Remote Sensing*, **10**, 751–761.

Qu, J. J., X. Hao, M. Kafatos, and L. Wang, 2006: Asian Dust Storm Monitoring Combining Terra and Aqua MODIS SRB Measurements. *IEEE Geoscience and Remote Sensing Letters,* **Vol. 3, No. 4**, 484-486.

RA II Pilot Project, 2011: Newsletter **Vol. 3 No.2**

Roskovensky, J. K., and K. N. Liou, 2005: Differentiating airborne dust from cirrus clouds using MODIS data, *Geophysical Research Letters*, **32**, L12809.

Simpson, J.J., Hufford, G., Pieri, D., Berg, J., 2000: Failures in detecting volcanic ash from a satellite-based technique, *Remote Sensing of Environment*, **72**, 191–217.

Tanré, D., Y. J. Kaufman, M. Herman, and S. Mattoo, 1997: Remote sensing of aerosol properties over oceans using the MODIS/EOS spectral radiances. *Journal of Geophysical Research,* **Vol. 102, NO. D14**, 16971-16988.

Tsunogai, S. and T. Kondo, 1982: Sporadic Transport and Deposition of Continental Aerosols to the Pacific Ocean. *Journal of Geophysical Research,* **87, NO. C11,** 8870-8874.

Yeo, H. G. and J. H. Kim, 2002: SPM and fungal spores in the ambient air of west Korea during the Asian dust (Yellow sand) period. *Atmospheric Environment*, **36**, 5437-5442.

Zhang, P., N. M. Lu, X. Q. Hu, and C. H. Dong, 2006: Identification and physical retrieval of dust storm using three MODIS thermal IR channels, *Global and Planetary Change*, **52**, 197-206.